DANISH METEOROLOGICAL INSTITUTE

SCIENTIFIC REPORT

03-19

Improved Models for Computing the Roughness Parameters of Urban Areas

D4.4 FUMAPEX Report

Editors: Alexander Baklanov, DMI
Sylvain Joffre, FMI

FUMAPEX Integrated Systems for Forecasting Urban Meteorology, Air Pollution and Population Exposure

Contract number: EVK4-CT-2002-00097

WP4: Improvement of parameterisation of urban atmospheric processes and urban physiographic data classification

Deliverable D4.4: October 2003

dmi.dk

COPENHAGEN 2003

ISSN: 0905-3263 (printed)
ISSN: 1399-1949 (online)
ISBN: 87-7478-495-1

Contents

Introduction

”Improvement of parameterisation of urban atmospheric processes and urban physiographic data classification” is the focus of the FUMAPEX workpackage 4 (WP4).

One of WP4 items is the improvement of the parameterisation of roughness parameters of urban areas through targeted measurements of meteorological parameters as well as the implementation and verification of the geometrical model for roughness parameters in urban areas.

As part of the strategy of NWP models ”urbanisation”, this report focuses on improvement of urban roughness characteristics’ calculations for urban-scale NWP models and consists of the Deliverable 4.4 ”Improved models for computing the roughness parameters of urban areas” as part of the WP4 activities of the FUMAPEX project.

The following FUMAPEX partners participated in this contribution/reporting work for WP4.4:

- Partner 1: Danish Meteorological Institute (DMI), Denmark (including Prof. S. Zilitinkevich and UCL, Belgium - as subcontractors);
- Partner 2: German Weather Service (DWD), Germany;
- Partner 3: Meteorological Institute of the Hamburg University (MIHU), Germany;
- Partner 4: Centro De Estudios Ambientales Del Mediterrano (CEAM), Spain;
- Partner 5: Ecole Centrale de Nantes (ECN), France;
- Partner 6: Finnish Meteorological Institute (FMI), Finland;
- Partner 16: Swiss Federal Institute of Technology (EPFL), Switzerland.

The report was written by A. Baklanov (Chapters 1, 3.1, 3.2, 3.3, 5), P. G. Mestayer, N. Long and A. Mahura (Chapter 2), S. Zilitinkevich and S. Joffre (Ch. 3.2), A. Clappier (Ch. 3.4), M. Schatzmann, M. Schultz and B. Leitl (Chapter 4).

1. FUMAPEX operational NWP models and strategy for their ”urbanisation”

written by Alexander Baklanov (DMI)

1.1. Existing level of ”urbanisation” in operational NWP models

As modern NWP models approach meso- and city-scale resolution (e.g. *Saito, 1998; LM, 1999; Sattler, 1999; Baklanov et al., 2002*) and utilize land-use databases with a resolution of 1 km or finer, the situation is changing nowadays. Hence, a revision of the conventional conception for urban air quality (UAQ) forecasting is required. Some European countries already made some progress in this direction and they are on a very promising path (*Clean City Air 1999; Kukkonen, 2001*).

The future possibilities of NWP models for urban air pollution forecasting are influenced by the following aspects:

- During the last decade, substantial progress in NWP modelling and the description of urban atmospheric processes have been achieved.

- Modern nested NWP models are approaching the meso- and city-scale resolution utilising land-use databases of 1 km resolution or finer.
- In combination with recent scientific developments in the field of urban atmospheric physics and enhanced availability of high-resolution urban surface characteristics, the capability of NWP models to provide high quality urban meteorological data will therefore increase.
- However, existing operational UAQ models often employ simple local measurements and meteorological pre-processors with a poor description of temporal and spatial evolution of meteorological variables on the urban scale.
- Modern UAQ models demand much more meteorological input data, such as humidity distribution, cloud characteristics, intensity and type of precipitation, radiation characteristics etc.
- Clearly, present UAQ models could greatly benefit from utilising meteorological data from NWP models to give a more physically consistent basis for urban air quality forecasts.

Despite the increased resolution of modern NWP models and various advantages mentioned above, existing operational NWP models have several shortcomings with respect to urban areas such as:

- In most operational NWP models, urban and non-urban areas are mostly described by similar sub-surface, surface, and boundary layer formulations.
- These formulations do not account for specific urban dynamics and energetics northeir impact on the intrinsic numerical simulation of the atmospheric boundary layer and its various characteristics (e.g. internal boundary layers, urban heat islands, precipitation patterns).
- Additionally, NWP models are not primarily developed for air pollution and emergency modelling, and their outputs need to be designed to suit as input for urban and meso-scale air pollution and emergency preparedness models.

In the FUMAPEX project the following NWP models (*Fay, 2003*) will be considered for ”urbanisation”:

1. DMI-HIRLAM (Partner 1: DMI);
2. LokalModell (LM) (Partner 2: DWD);
3. MM5 (Partner 9: DNMI (met.no)); => WRF (?)
4. RAMS (Partner 4: CEAM).

Moreover, three additional research meso-scale meteorological models of FUMAPEX partners are already used for testing improved urban parameterisations:

1. SUBMESO LES Model (Partner 5: ECN);
2. Finite Volume Model, FVM (Partner 16: EPFL);
3. Topographic Vorticity-Mode Mesoscale (TVM) Model (Guy Schayes, UCL, subcont. of DMI).

1.2. Strategy for urbanisation of NWP models in FUMAPEX

In a general sense, the following urban ***features*** can influence the atmospheric flow, urban microclimate, turbulence regime and, correspondently, the transport, dispersion, and deposition of pollutant or radioactive releases within the urban areas:

- Local-scale non-homogeneities, sharp changes of roughness and heat fluxes;
- Wind-velocity reducing effects due to buildings;
- Redistribution of eddies, from large to small, due to buildings;
- Trapping of radiation in street canyons;

- Effect of urban soil structure, diffusivities of heat and water vapour;
- Anthropogenic heat fluxes, including the so-called urban heat island (UHI);
- Intrinsic urban internal boundary layers (IBL) and urban mixing height (MH);
- Effects of pollutants (including aerosols) on urban meteorology and climate;
- Urban effects on clouds and precipitation (enhanced cloud condensation nuclei number but with altered size-distribution).

Accordingly, considering the mentioned above features, the following ***consideration*** of urban effects in the improved urban-scale NWP models should be implemented:

- Higher spatial grid resolution and model downscaling;
- Improved physiographic data and land-use classification;
- Calculation of effective urban roughness;
- Calculation of urban heat fluxes;
- Urban canopy sub-model;
- Simulation of the internal boundary layers and mixing height in urban areas;
- Urban measurement assimilation in NWP models.

At the current stage, although operational NWP models do not consider those features and aspects and do not include most of potential urban improvements, there are significant scientific developments in the field of urban atmospheric physics and enhanced availability of high-resolution urban surface characteristics.

Existing approaches for the specific treatment of urban boundary layer features include the following ***achievements***:

- Urban roughness effects (e.g., *Bornstein, 1975, 2001; Hunt et al., 2003*)
- Urban surface energy balance (*Oke et al., 1999, Piringer et al., 2002*)
- Town Energy Balance (TEB) scheme (*Masson, 2000*)
- Urban surface exchange sub-layer model (*Martilli et al., 2002*)
- SM2-U urban area soil submodel (*Mestayer et al., 2002*)
- Prognostic models for UBL height (*Zilitinkevich & Baklanov, 2002; Gryning & Bartchvarova, 2002*).

Implementation of the above mentioned features and aspects in NWP models is very ambitious and time-consuming. Therefore, at first, within the scope of the FUMAPEX project, we consider three main steps or levels of complexity of the "***NWP urbanisation***" (*Baklanov, 2003*):

1. Simple corrections to the surface roughness for urban areas, e.g., following *Grimmond & Oke (1999)*, and heat fluxes (adding the albedo changes and additional urban heat flux, e.g. via heat production in the city) within the existing non-urban physical parameterisations of the surface layer in the model with higher resolution and improved land-use classification. It is realised in the DMI-HIRLAM model.

2. Improvement and realisation of a new flux aggregation technique, suggested by the Risø National Laboratory in cooperation with DMI (*Hasager et al., 2003*), for urban areas. Recently, this module was implemented in the DMI-HIRLAM model for non-urban areas. The approach can be extended to urban canopies as well. However, experimental data are needed to verify these parameterisations for urban areas.

3. Implementation of special physical parameterisations for the urban sub-layer into the NWP models. In this project we plan to incorporate a new urban module developed in FUMAPEX into both HIRLAM and LM models and based on the following two different urban submodels:

(i) Urban surface exchange parameterisation, developed by the Swiss team, Partner 16 (the model description is given by *Martilli et al., 2002*);

(ii) SM2-U urban area soil submodel, developed by the French team, Partner 5 (the model description is given by *Dupont et al., 2002*).

The main problems to improve the NWP models for the urban scale are the following:

- Nested high resolution, urban scale resolved models; coupling atmospheric mesoscale models with heterogeneous chemistry and aerosol models.
- Improvement of the urban boundary layer parameterisation, e.g. turbulent sensible and latent heat fluxes, revised roughness and land-use parameters and models.
- Assimilation of surface characteristics based on satellite data and additional urban meteorological measurements for the NWP models.
- Model interface capable to connect meso-scale meteorological model results to updated UAQ and atmospheric chemistry models.
- Improved integrated urban meteorology, air pollution and population exposure modelling system suitable for application in any European urban area on the basis of available operational weather forecast.
- Evaluation and sensitivity studies of these improvements on the meteorological input fields for UAQ models and resulting air quality simulations.

The scheme of suggested improvements of meteorological forecasts in urban areas and interfaces to UAQ models for the UAQIFS and emergency preparedness systems is shown in Fig 1.2.1.

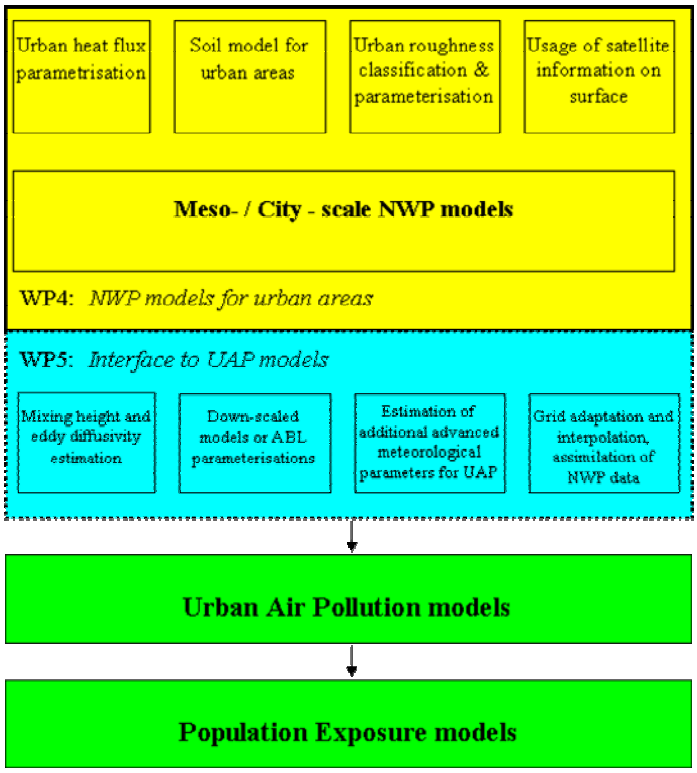

Fig 1.2.1. Scheme of the suggested improvements of meteorological forecasts (NWP) in urban areas and interfaces to UAP models for the Urban Air Quality Information Forecasting Systems.

1.3. Improvement of spatial resolution and roughness calculation

1.3.1. Increased grid resolution and nesting of NWP models

The growth of computer power and implementation of grid nesting techniques allowed modern NWP models to approach the resolution of the city-scale (*Baklanov et al., 2002*).

For example, the Danish operational system (*Sass et al., 2002*) consists of several nested models named DMI-HIRLAM - ”G”, ”N”, ”E”, and ”D” versions. The high resolution model ”D”, covering an area around Denmark, has 5 km horizontal grid and uses boundary values from the large scale model ”E”. During the last year, DMI started to run an experimental “I”-version of DMI-HIRLAM over Denmark, including the city of Copenhagen, with a horizontal resolution of 1.4 km. The vertical resolution was increased up to 52 vertical levels (60 levels proposed starting from year of 2004). Improvements of the parameterizations for urban atmospheric processes and urban physiographic data classification, following the first approach, were realised in this version. Some examples of forecasted wind fields at 10 meter height and air temperature at 2 meter for the Copenhagen metropolitan area are presented in Fig 1.3.1.1.

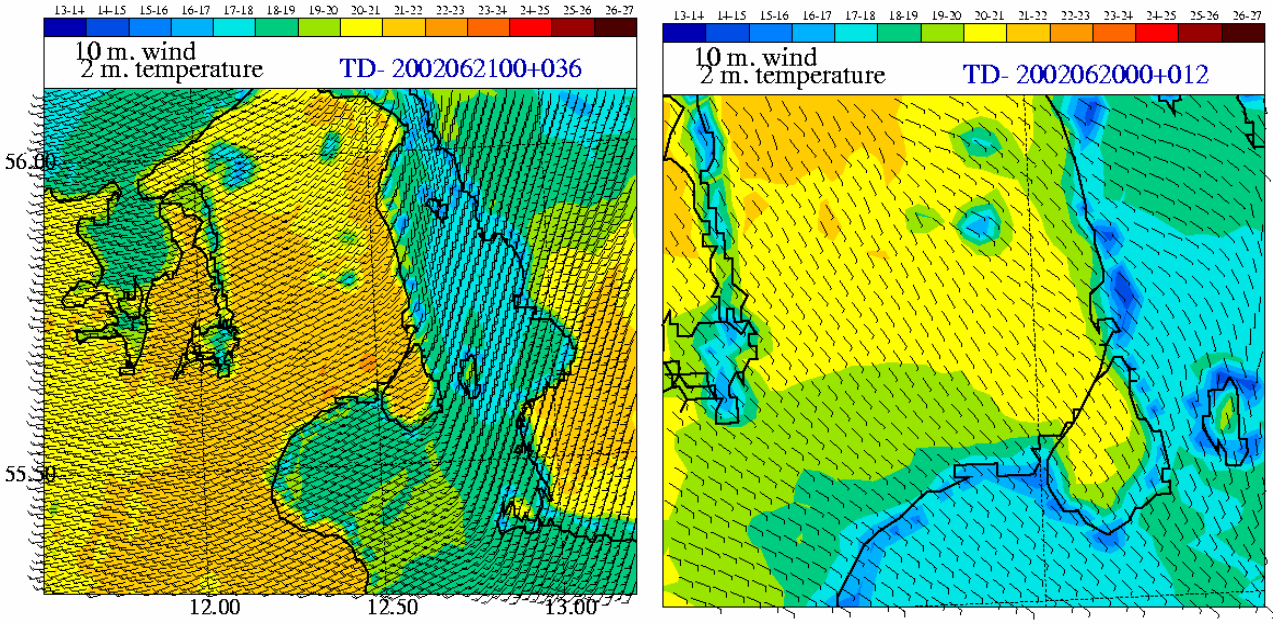

Fig 1.3.1.1. Forecasted wind and air temperature fields at 10 and 2 m, respectively, for the Copenhagen metropolitan area by experimental “I”-version of DMI-HIRLAM with horizontal resolution of 1.4 km.

The German DWD Local Model (LM) (*Doms and Schättler, 1999*) is currently operated as a nest within the Global Model (GME). LM has a resolution of 7 km for the Central and Western Europe, and starting year of 2003, it became operational for that area with a resolution of 2.8 km. In the framework of the European non-hydrostatic modelling consortium COSMO, triple nesting of LM will be realised to produce weather forecasts for the Olympic games in Athens (year of 2006) on a 1.1 km grid and for other possible purposes (such as airports, cities, etc.).

Since year of 2000, DWD developed and operated the stand-alone NWP model chain comprising the Global Model with about 60 km mesh size (triangular grid), 31 vertical levels, and full data assimilation. It provides initial and boundary values to the nested non-hydrostatic LM with 7 km and 35 levels operational resolutions for the Central and Western Europe.

The growth of supercomputer power (new IBM RS6000) will allow increased resolution for both GME and LM models. The pre-operational LM version has 43 vertical levels and 2.8 km horizontal resolution and will be run for nowcasting purposes for Germany, while the area of the operational 7 km version will be extended across most of Europe. In FUMAPEX, the horizontal and vertical resolutions of LM may now be increased as desired after the finalisation of the 1-way self-nesting version of LM (*Fay, 2003*). This version was already distributed to Partner 8, and partners of the COSMO consortium. Preliminary modelling of two stable winter inversion episodes for Oslo and Helsinki was performed in the framework of COST715 with a 2-way interactive LM nesting version which is under development in COSMO.

A research high-resolution version of the LM (the LLM) was developed at DWD (*Herzog et al., 2002a; 2002b*). It has a resolution of 100 m, 39 layers (up to 3 km height), 3D turbulent fluxes, and parameterisation of subgrid-scale turbulence including the prognostic fully 3D TKE equation. The model is driven by local measurements (also LM-derived input data), uses subgrid-scale land-use and orography databases and, at the moment, is applied for the rural environment of the East German DWD research observatory Lindenberg. The FUMAPEX Partner 8 (ARPA) is interested in using the model for the city of Bologna applications, but the intended application had to be suspended for resource reasons. Some recent and future activities at the DWD include:

- Introduction of prognostic turbulence scheme of level 2.5 Closure (*Mellor & Yamada, 1974; Raschendorfer, 1999);*
- Pre-operational testing of a new 7 layer soil model;
- Pre-operational testing of increased resolution for NWP models;
- Preliminary urban episode modelling in COST-715.

At DNMI, the non-hydrostatic MM5 model (*Grell et al., 1995*) is nested with HIRLAM (*Berge et al., 2002).* The HIRLAM model is operated on a 10 km horizontal resolution for the North-West Europe. A domain with a resolution of 3 km has been set up for the city of Oslo region in which MM5 is one-way nested with HIRLAM. A two-way nesting takes place between domains of 3 km vs. 1 km resolutions covering the city of Oslo. The output data from MM5 are employed to the Air Quality Model developed by the Norwegian Institute for Air Research (NILU). The model was run daily for a period starting from 1 Nov 2000 to 1 May 2001, which is a season of the largest air quality problems in Oslo. For the winter 1999/2000 the model was run for 22 days (see *Clean City Air, 2000; Berge et al., 2002*). An evaluation of the meteorological predictions was made based on this dataset.

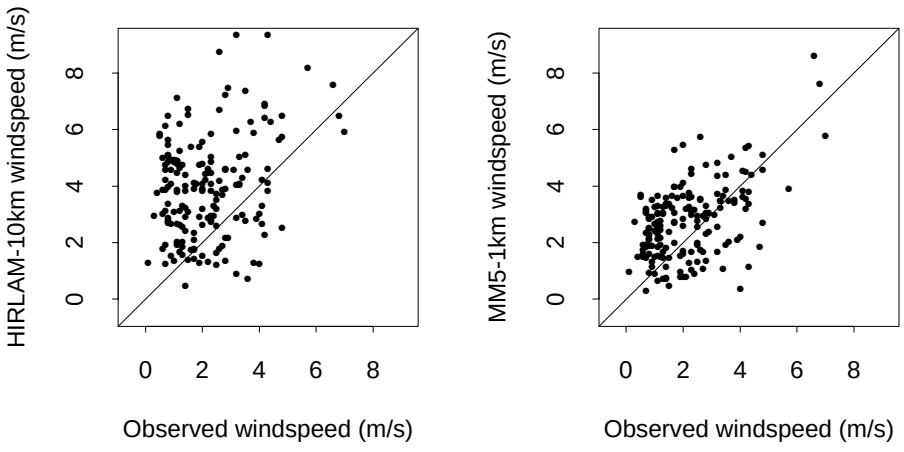

Fig 1.3.1.2. Observed and modelled wind speeds at Valle Hovin, meteorological station in Oslo, for 22 days during winter of 1999/2000.

In Figure 1.3.1.2 the wind speed predictions at 25 m from HIRLAM with 10 km resolution and MM5 with 1 km resolution are compared with measurements from a wind mast. We clearly see that the wind speed predictions are considerably improved employing the MM5 (1 km) vs. HIRLAM (10 km). A clear improvement was also found for predictions of wind direction (*Berge et al., 2002*). Since the complex topography in the Oslo region has a great impact on the local winds, we would ascribe a large part of this improvement to the increased horizontal resolution. However, some of the improvements may also be due to differences in model formulations. The latter has not been yet investigated and it would require a set-up of the HIRLAM model on a 1 km horizontal grid for the Oslo region. However, for the temperature predictions (not shown), the strength of the near surface inversion is somewhat overestimated by MM5 (as well as HIRLAM). Studies have been undertaken to improve this, and a first order PBL-closure scheme has been modified in order to give a better description of the near surface temperature profiles during stable conditions (*Sorteberg, 2001*).

1.3.2. Roughness calculation in operational NWP models

The results of existing NWP models will only be reliable for urban- and mesoscales when refined databases for external parameters with 1 km resolution or finer are also provided and used.

Utilising such land-use databases, models can reach a detailed description of surface features, including the identification of urban areas. The DMI-HIRLAM model uses a land-use classification with 1 km resolution from the Global Land Cover Characteristics data (GLCC) and Danish KMS data and could be improved down to 250 meters. The database describes 21 types of land cover including a separate class of urban areas (*Sattler, 2000*), see Tab. 1.3.2.1 and Fig. 1.3.2.1. Each model grid cell includes a percentage of different classes in the cell. Thus urban areas are presented differently in a city centre vs. suburban territories. Fig. 1.3.2.2 shows presentation of the urban surface percentage in each computing grid cell (1.4 x 1.4 km) for the urban-scale experimental version of DMI-HIRLAM for the Copenhagen metropolitan area and Øresund region.

Tab 1.3.2.1. Land-use categories in DMI-HIRLAM (from *Sattler, 2000*).

Class #	***Description of the land-class***	11	Semi-desert
1	Crops, Mixed Farming	12	Ice Caps and Glaciers
2	Short Grass	13	Bogs and Marshes
3	Evergreen Needle-leaf Trees	14	Inland Water
4	Deciduous Needle-leaf Tree	15	Ocean
5	Deciduous Broad-leaf Trees	16	Evergreen Shrubs
6	Evergreen Broad-leaf Trees	17	Deciduous Shrubs
7	Tall Grass	18	Mixed Forest
8	Desert	19	Interrupted Forest
9	Tundra	20	Water and Land Mixtures
10	Irrigated Crops	21	Urban area

Correspondingly, the surface parameters in NWP models, like the albedo, surface fluxes, and roughness length (z_0) are simulated from high resolution physiographic data. However, in the operational DMI-HIRLAM model the roughness length is obtained from a table of the land-use classes with corresponding values of z_0 for each class and simulated climate generation fields, and is recalculated due to the percentage of each land-use class in the grid-cell (*Sattler, 1999*).

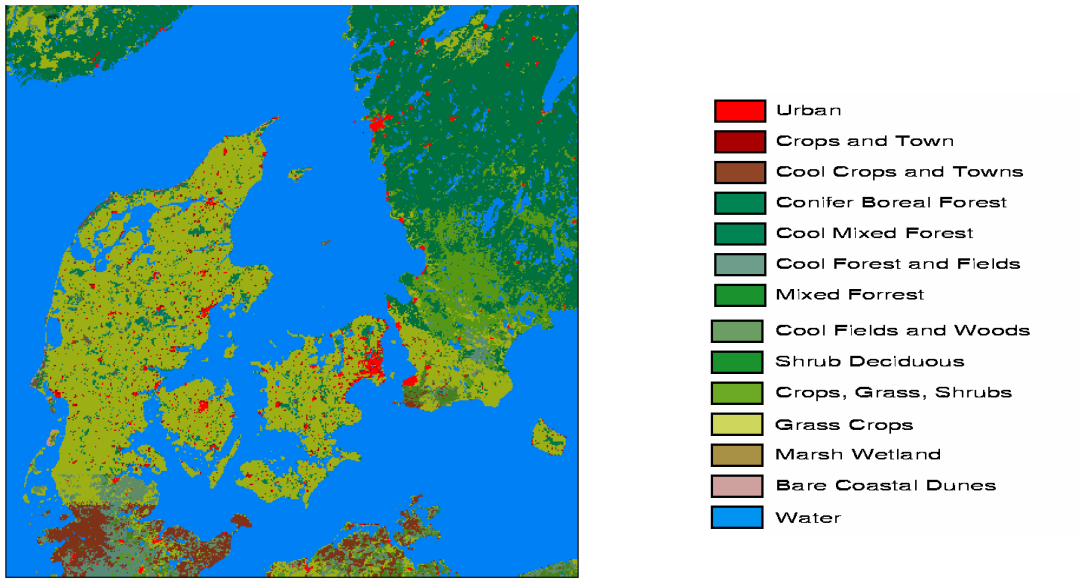

Fig. 1.3.2.1. Land-use classification over Denmark and south Sweden from GLCC- and KMS-data for the DMI-HIRLAM-D model with 1 km resolution (*Sattler, 1999*); the legend below includes types of land/sea including one class of urban areas.

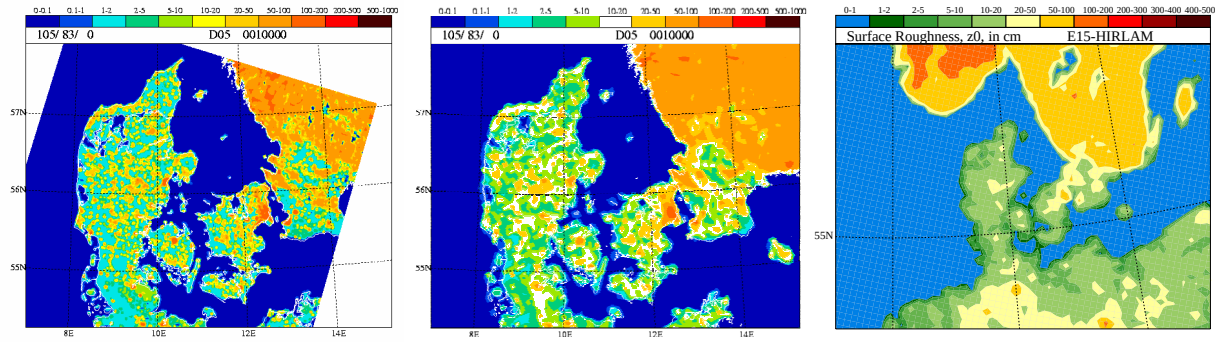

Fig. 1.3.2.2. The simulated roughness length (z_0) for Denmark from the high resolution physiographic data for DMI-HIRLAM versions: "I" of 1.5 km resolution (left), "D" of 5 km resolution (middle), and "E" of 15 km resolution (right).

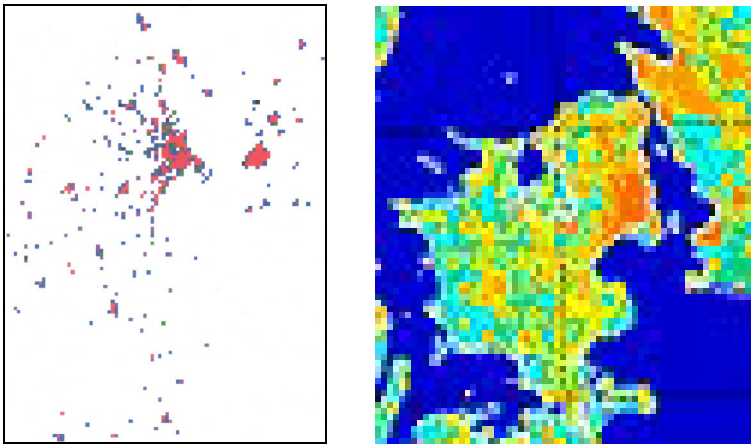

Figure 1.3.2.3. Mapping of the urban surface percentage in each computing grid cell urban surface percentage (left) and roughness length (right), simulated in the urban-scale DMI-HIRLAM "I"-version (1.4 km) for the Copenhagen metropolitan area and Øresund region.

Fig. 1.3.2.2 shows the roughness length, simulated in different DMI-HIRLAM versions: for Denmark in 1.4 km (left) and 5 km (middle) resolutions, and for the European territory in 15 km resolution (right). Fig 1.3.2.3 shows the urban surface percentage (left) and roughness length (right), simulated in the DMI-HIRLAM "I"-version (1.4 km) for the Copenhagen Metropolitan area and Øresund region.

For application of the DWD Local Model versions for the urban scale, the external parameters with a resolution of 1 km or finer are needed. However, there is no the urban category in the land-use classification used in the operational version of the LM model. Fig. 1.3.2.4 presents the roughness length for the central European territory, simulated in the LM with 7, 2.8, and 1.1 km resolution (all based on 1 x 1 km database). z_0 not only shows much more details (valleys, etc.), but also decreases with increasing resolution, because the subscale orographic influence decreases with increased NWP model resolution, whereas the portion of the plant cover stays approximately the same. However, with 1.1 km resolution map (in Fig. 1.3.2.4) the limitations of using the common 1 x 1 km database become apparent: z_0 appears too low, especially, in mountainous areas due to the absent roughness in the sub-grid scale of the database (which has a resolution close to the accuracy of the calculated field) (*Baklanov et al., 2002*).

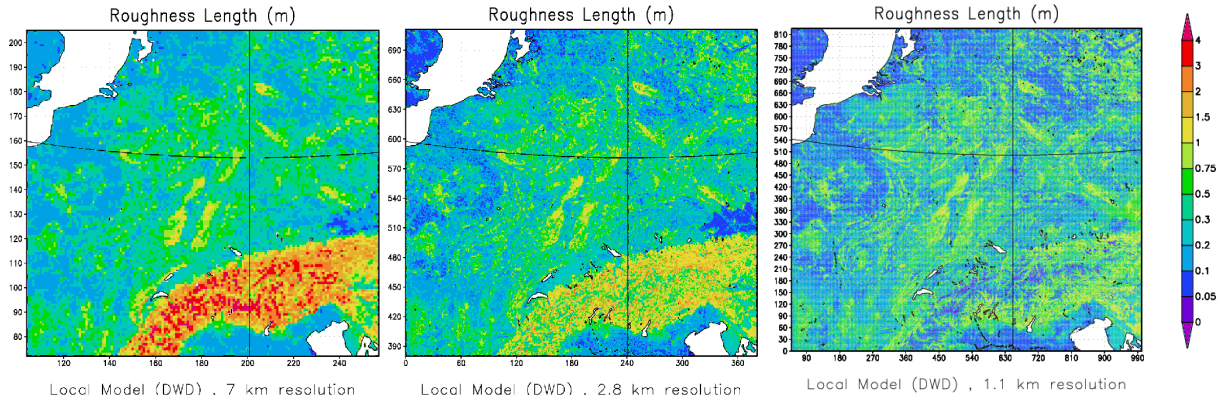

Fig. 1.3.2.4. DWD Local Model simulation of the roughness length in 7 (left), 2.8 (middle), and 1.1 (right) km resolutions (all based on 1 x 1 km database).

Partner 4 (CEAM) upgrades the model RAMS (*Pielke et al., 1992*) considering the effect of meso-scale over the PBL properties at urban scale, in particular for Mediterranean cities. They have incorporated into the RAMS model the SST data obtained from an algorithm based on NOAA satellite high-resolution images (*Badenas et al., 1997*). The land categories (from the CORINE and PELCOM datasets) following USGS categories have been reclassified. CEAM also has inter-compared the different reclassified datasets, finding significant differences.

As a current step in FUMAPEX CEAM realises the following in this field:

- To incorporate into the RAMS model the reclassified CORINE and PELCOM datasets;
- To perform a sensitivity analysis of the improved model performance by means of modelling 1-2 scenarios/episodes (for 1-2 Mediterranean cities).

This improved model performance lies on the:

- Incorporation of a more accurate SST for each scenario/episode;
- Incorporation of the new land datasets (CORINE+PELCOM);
- Definition of optimum domains, grid sizes and temporal resolutions to account for atmospheric drive forces (for each city).

2. Parameterizations for roughness parameters in urban areas

by Patrice G. Mestayer, Nathalie Long, Alexander Mahura (ECN)

Over the dense canopy of city centers, the momentum flux computation in numerical models requires the development of new parameterizations. These should account not only for the local building layout, but also for its thermal structure and size of the "urban patch". Such advanced parameterizations are not yet available. Therefore, our numerical models use the same wall laws for urban surfaces as those that are common for natural surfaces. In fact, it is assumed that the equilibrium constant flux relationships are not too erroneous at the level z_s where the wall law is applied. Usually this is the boundary between the first and second grid mesh layers. The optimal choice of z_s is being still an open question. Assuming that at this level the turbulent boundary layer is fully developed and in an equilibrium state, the wall law can be derived from the logarithmic profile relationship:

$$U_h(z_s) = \frac{u_{*s}}{\kappa} \ln\left(\frac{z_s - z_d}{z_0} - \Psi_m\left(\frac{z_s}{L}\right)\right) \tag{2.1}$$

where:

$U_h(z_s)$ - horizontal velocity component,

$u_{*s} = \left(-\overline{u'w'(z_s)}\right)^{1/2}$ – friction velocity,

κ - von Karman constant,

$\Psi_m\left(\frac{z_s}{L}\right)$ - stability correction function,

L - Monin-Obukhov length.

$U_h(z_s)$ and u_{*s} are obtained from the computation of the Navier-Stokes equations at the previous time step. This computation requires the values of the roughness length z_o and displacement height z_d at grid cell. Let us summarize methods allowing to evaluate both z_o and z_d values for urban terrain/canopy with a fine spatial resolution.

2.1. Wind and land-use based methods

Two types of methods can be employed to determine z_o and z_d in urban areas as discussed by *Grimmond & Oke (1999)*. The first methods are wind based (also referred as micrometeorological or anemometric), and the second methods are land-use based (morphometric or geometric).

The wind-based methods are empirical, and they can take into account the influence of wind direction. But a shortcoming is that for a full city an enormous amount of measurements is required. These methods assume the logarithmic wind profile and use the Monin-Obukhov similarity theory and stability functions, which further assume a horizontal homogeneity. The latter is quite an important restriction. *Bottema (1997)* argued that over town centers, the minimum fetch for homogeneity may be in excess of 2 km. *Grimmond et al. (1998)* distinguished between methods using slow– and fast–response anemometry as well as measurements at several or only one level. These methods allow to evaluate u_{*s}, z_o, and z_d separately or in combination, and thus they have different levels of accuracy. For urban sites, *Rotach (1994)* adapted a method derived from *Tillman*

(1972) to determine the displacement height z_d from measurements of temperature variance σ_θ, independently of z_o, considering that $\frac{\sigma_\theta}{\theta_*}$ varies as $\frac{z_s - z_d}{L}$ to the power –⅓, such as, e.g. :

$$\frac{\sigma_\theta}{\theta_*} = -C_1\left(C_2 - \frac{z_s - z_d}{L}\right)^{-1/3}, \qquad \theta_* = \frac{\overline{w'\theta'}}{u_*} \tag{2.2}$$

where: θ_* - Monin-Obukhov temperature scale. *Grimmond et al. (1998)* tests vs. experimental data did not support this method. For several sites this method did not provide reliable values of z_d, while for others it was very sensitive to the form of the empirical function and values of coefficients.

The land-use methods, on the other hand, may provide estimations of the "intrinsic" roughness parameters of small "urban patches" or urban districts. One weakness of this method is the fact that generally validation can be done only with idealized building layouts in wind tunnels. Another weakness is the lack of a direct momentum flux estimates. If the patches are too small to assume homogeneity, the advanced flux parameterizations will be needed.

Let us further distinguish between the morphometric and morphologic methods. The morphometric methods require computation of geometric parameters from a statistical analysis of urban databases. The morphologic (classification) methods rely upon the visual observation/inspection of urban databases or aerial photography.

Since the experimental documentation of z_o and z_d distributions for a whole urban area does not appear to be a feasible task, the land-use methods seem to be only a way in mapping of these parameters for further numerical simulations of the urban atmospheric boundary layer. The methods require some analysis of urban databases describing not only the land-use, but also shapes, sizes, and arrangements of the roughness elements composing the urban canopy, buildings and trees.

2.2. Morphometric methods

Figs. 2.2.1-2.2.2, adapted from *Bottema (1997)*, define the notation of building dimensions and inter-spaces for regular building arrays. Wind direction is equal to 0° if wind is perpendicular to the longer building face, or in direction of the largest inter-spaces d_x or d_y if $\frac{L_x}{L_y} = 1$. The regular building arrays can be considered as "normal" (Fig. 1) or "staggered" (i.e. when buildings of one row face building separations of the next row; as shown in Fig. 2).

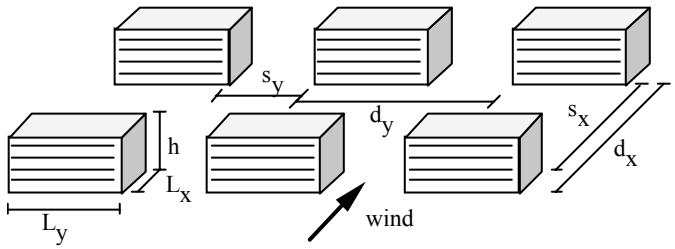

Fig. 2.2.1. Definition of geometrical parameters in regular building arrays.

In reality, of course, the building arrays as well as the sizes of the individual building are not the same. For simplicity, the same notations for identical and non-identical building arrays are kept,

and so, it can be written:

$$\sum \beta\gamma \quad \text{for} \quad \sum_{i=1}^{Nb} \beta_i \gamma_i$$

where γ_i, β_i are the individual building sizes, and *Nb* the number of buildings in the considered area.

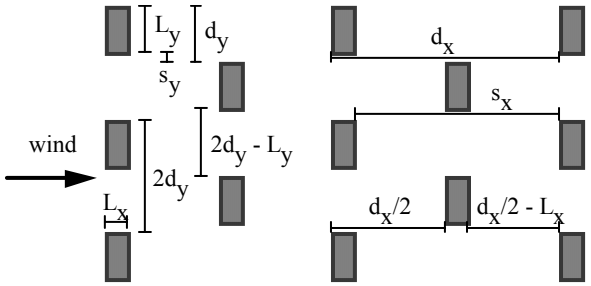

Fig. 2.2.2. Definition of geometrical parameters in staggered building arrays.

Following the model reviews of *Grimmond & Oke (1999)* and *Mestayer (1998)*, at first let us consider models that take into account only the mean height of obstacles *h:*

$$z_0 = \alpha_0 h, \qquad z_d = \alpha_d h, \tag{2.3}$$

where: α_0, α_d coefficients are constants, and $\alpha_0 = 0.142$ (*Paeschke, 1938*), 0.111 (*Stull, 1988*), 0.1 (*Oke, 1978; 1987*); and $\alpha_d = 0.667$ (*Oke, 1978; 1987*), 0.75 (*Thom, 1971; Rotach 1993*), etc. [these references can be found in *Grimmond & Oke, 1999*]. After experimental survey, as a "rule of thumb", *Grimmond & Oke (1999)* proposed: $\alpha_0 = 0.1$ and $\alpha_d = 0.5$, which are also recommended values of *Hanna & Chang (1992)*, or $\alpha_d = 0.5$, 0.6, and 0.7 for the low–, medium-, and high–density urban sites, respectively.

Kutzbach (1961) and *Counihan (1971)* introduced the α coefficients that depend on the plan building density or fraction of built-up area λ_p, which is defined as followed:

$$\lambda_p = \frac{\sum L_x L_y}{\sum d_x d_y}. \tag{2.4}$$

Their empirical determinations of the α-λ_p relationships, employing wind tunnel measurements, were not in a good agreement with each other. *Grimmond & Oke (1999)* demonstrated that the Kutzbach's method provided reasonable estimates only for the low λ_p ratios, but it constantly failed to give reasonable values for real cities, while the Counihan's method is more applicable in theory for the higher values, but it often fails too because actual λ_p values are outside of the range of applicability.

Kondo & Yamazawa (1986) proposed a quite similar relationship where the mean building height is an area weighted mean:

$$z_0 = \frac{1}{4}\frac{\sum hL_x L_y}{\sum d_x d_y}. \qquad (2.5)$$

Grimmond & Oke (1999) noted that this model predicted continuously increasing values of $\frac{z_0}{h}$ with λ_p in contrast with Counihan's results showing a decrease of $\frac{z_0}{h}$ for λ_p > 30%, and in contradiction with their "simple heuristic argument": when the roughness element density increases, so does the roughness of the system, up to the point where adding new elements reduces the effective drag of those already present, since the new elements increase the mutual sheltering (Fig. 2.2.3).

Publications indicating the range of λ_p values that can be found are rare. *Soliman (1976)* presented an overview graph for different densities of different districts (probably rather recently built in North-Western Europe). This graph showed that λ_p ranges between 5 and 50%. The densities below 10% coincided often with high-rise buildings (> 10 stores), while for the higher densities there is no obvious relationship between building height and building density. *Grimmond & Oke (1999)* noted that real cities show λ_p between 19 and 63%, and z_o peak lies between 30 and 40%.

For estimation of z_o, λ_p is not the best parameter. Because z_o is closely related to τ (the wind drag on obstacles) divided by a representative ground area, a more representative parameter is the frontal density ratio λ_f, which refers to the surface area facing the wind:

$$\lambda_f = \frac{\sum hL_y}{\sum d_x d_y}, \qquad (2.6)$$

and thus λ_f is a function of wind direction. The first model using λ_f was derived by *Lettau (1969)* from wind profiles over bushel baskets on the frozen lake Mendota:

$$\frac{z_0}{h} = \frac{1}{2}\lambda_f. \qquad (2.7)$$

Unfortunately, this expression cannot be valid for all geometries and densities, and especially the highest ones, since it lacks the effect of mutual sheltering. Furthermore, *Businger (1975)* extended the Lettau's formula by assuming that only part of the obstacles with $z > z_d$ counted as the effective frontal surface generating drag. He wrongly assumed this to be proportional to $(h - z_d)^2$ instead of $L_x(h - z_d)$. Nevertheless a formula for shelterbelts of infinite width was proposed:

$$\frac{z_0}{h} = \frac{1}{2}\frac{h}{d_x}\left(1 - C_2\frac{h}{d_x}\right)^2. \qquad (2.8)$$

It was the first model where, for high densities, z_o decreases due to the effect of mutual sheltering (although it leans heavily on the presumed validity of Lettau's formula).

Raupach's (*1992; 1994; 1995*) work represented a major step forward in deriving physically based models of the roughness parameters. The random-sparse-canopy model was proposed. It was based on a detailed analysis of the effective shelter areas and volumes, and on the partition between surface shear stress and obstacle drag over surfaces presenting several types of roughness elements. For urban areas this model can be valid only for small and moderate building densities and for random arrangements of uniform buildings. It is summarized below, but best understood by first

following Bottema's (*1996; 1997*) rationale for the development of his complete urban roughness model.

First, it should be noted that z_o is actually a measure of the wind drag integral over the ground and obstacles, as shown by rewriting the equilibrium equation (1), and neglecting $\Psi_m\left(\frac{z}{L}\right)$ near the ground surface. This allows to relate z_o to the drag coefficient C_d at a given reference height z_{ref}:

$$C_d(z_{ref}) = \frac{\tau}{a_1 \rho_a U(z_{ref})^2} = 2\frac{u_*^2}{U(z_{ref})^2} = 2\left(\frac{\kappa}{\ln\left(\frac{z_{ref} - z_d}{z_0}\right)}\right)^2, \tag{2.9}$$

where a_1 is an experimental coefficient, which is in laboratory fluid mechanics usually considered equal to ½, but in the atmospheric science the value 1 is more suitable.

As a first approximation, it might be assumed by neglecting the inter-space surface stress that in practice the drag is essentially due to the building wakes. Assuming the validity of the equilibrium relationships at $z = h$, the reference height can be replaced by the mean building height h, to obtain :

$$\frac{z_0}{h} = \frac{h - z_{d,pl}}{h}\exp\left(-\frac{\kappa}{\left(\frac{1}{2}\lambda_f C_{dh}\right)^{1/2}}\right) \tag{2.10}$$

where: C_{dh} - unit building drag coefficient, and z_d is replaced by $z_{d,pl}$ (displacement height in the building median plane, i.e. the theoretical value of z_d if the buildings were of infinite length). This intermediate parameter is a measure of the sheltering effect of one building on its downwind neighbour, rather than of the overall upward flow displacement z_d. The calculated $z_{d,pl}$ values take into account the volumes of buildings themselves, and the volumes of their recirculation zones, as observed by several experimenters in wind tunnels (Fig. 2.2.3).

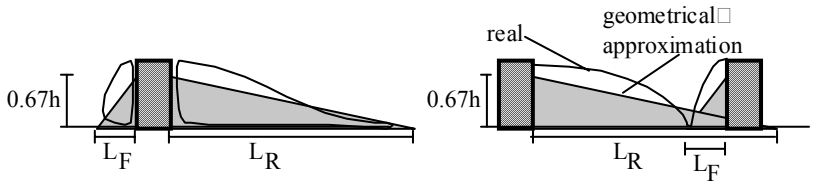

Fig. 2.2.3. Sketch of flow recirculation zone behind an isolated building and between two parallel buildings, showing real shape and geometrical approximation used in z_d formulas.

Bottema (1996; 1997) proposed different formulas separated according to the building arrangement, streamwise and lateral densities

For normal arrays, $\frac{z_d}{z_{d,pl,n}} = \frac{L_y}{d_y}$ and:

$$\frac{z_{d,pl,n}}{h} = \frac{L_x + \frac{1}{3}(L_R + L_F)}{d_x} \qquad for \qquad s_x > L_R + L_F, \tag{2.11a}$$

$$\frac{z_{d,pl,n}}{h} = \frac{L_x + \frac{1}{3}\left(2 - \frac{s_x}{L_R + L_F}\right)s_x}{d_x} \qquad for \qquad s_x < L_R + L_F. \tag{2.11b}$$

For staggered arrays, different formula was proposed in the earlier publications. *Bottema (1997)* showed that the same formula can be used for $\frac{z_{d,pl,s}}{h}$ if follow a new definition of the geometrical parameters given by Fig. 2.2.3. Yet, for very dense staggered arrays, when $s_y < L_y$, one building row partially shelters the following two rows. Then $z_d = z_{d,pl,d}$ and:

$$z_{d,pl,d} = z_{d,pl,s}\left(\frac{2s_y}{L_y} - 1\right) - z_{d,pl,n}\left(\frac{2 - 2s_y}{L_y}\right), \tag{2.12}$$

while this "double sheltering" also affects z_0 such that λ_f must be replaced by $\frac{s_y}{L_y}\lambda_f$ in (10):

$$\frac{z_0}{h} = \frac{h - z_{d,pl}}{h}\exp\left(-\frac{\kappa}{\left(\frac{1}{2}\left(\frac{2s_y}{L_y} - 1\right)\lambda_f C_{dh}\right)^{1/2}}\right) \tag{2.13}$$

For the values of C_{dh}, L_R and L_F in (10)-(13), *Bottema (1997)* recommended:

$$C_{dh} = 1.2\max\left(1 - 0.15\frac{L_x}{h}, 0.82\right)\min\left(0.65 + 0.06\frac{L_y}{h}, 1.0\right), \tag{2.14}$$

$$L_R + L_F = \frac{4L_y}{1 + \frac{L_y}{2h}}. \tag{2.15}$$

Fig. 2.2.4 shows the behaviour of $\frac{z_0}{h}$ as a function of the frontal density λ_f, and the model sensitivity to the geometrical parameters.

Considering that actual building arrangements, for urban map constructions *Bottema &*

Mestayer (1998) used a simplified power law model (initially proposed by *Bottema, 1995*) based on extensive analyses of the detailed model (10-15) around $\frac{L_x}{h} = 1$:

$$\frac{z_d}{h} = \lambda_p^{\,0.6} \text{ with relation (10) for } \frac{z_0}{h}. \tag{2.16}$$

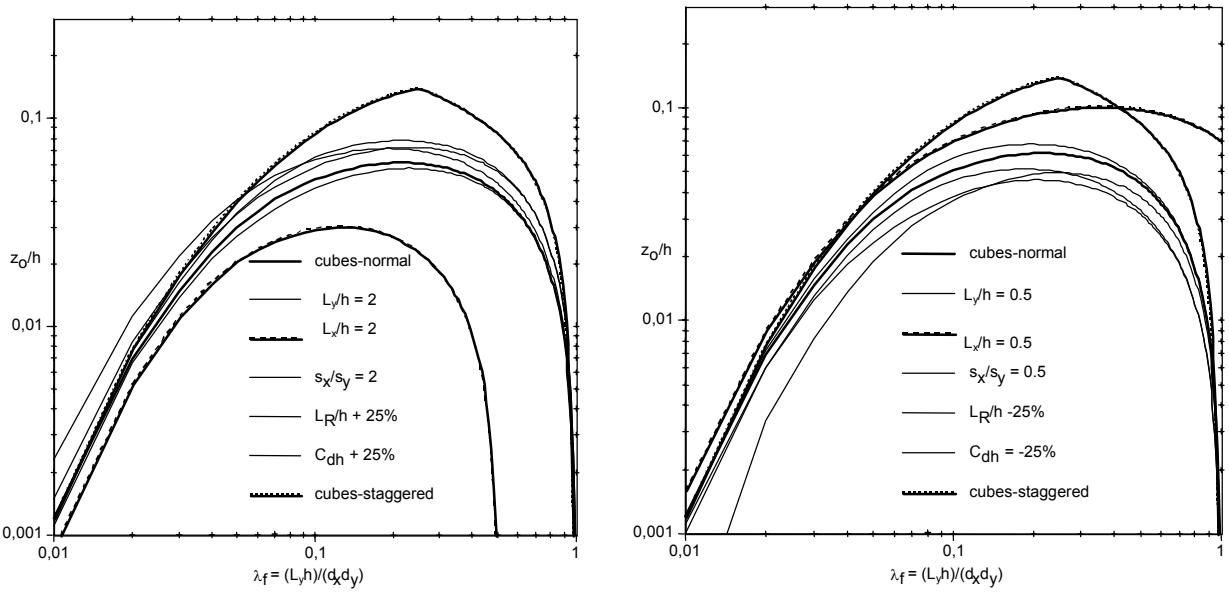

Fig. 2.2.4. The dependence of the roughness length on the mean building height and frontal density in regular arrays of square buildings. The light lines indicate the effect of increasing (left) and decreasing (right) of the geometrical parameters by a factor 2, and C_{dh} and $L_R + L_F$ by 25% (*Bottema, 1997*).

The presence of trees may be also taken into account, weighting their influence by their area density and porosity. The simplified model (10, 16) then becomes:

$$\frac{z_d}{h} = \left(\lambda_{pb} + (1-p)\lambda_{pt}\right)^{0.6}, \tag{2.17a}$$

$$\frac{z_0}{h} = \frac{h - z_d}{h} \exp\left(-\frac{\kappa}{\left(\frac{1}{2}\sum_b C_{db}\lambda_{fb} + \frac{1}{2}\sum_t (1-p) C_{dt}\lambda_{ft}\right)^{1/2}} \right), \tag{2.17b}$$

where: C_{db} and C_{dt} are the unit drag coefficients for buildings and trees, respectively; C_{db} is obtained from relation (14); and $C_{dt} = (1-p)C_{db}$. Tree porosity p varies between 0.2 and 0.6. These formulas for trees were first implemented and tested by *Bottema et al. (1998).*

The model constructed by *Raupach (1992, 1994, 1995)* may be summarized in the following way. Raupach also assumed that relation (1) is valid at $z = h$, thus obtaining:

$$z_0 = (h - z_d) \exp\left(-\frac{\kappa U(h)}{u_*} - \Psi_{RSL} \right), \tag{2.18}$$

where: Ψ_{RSL} is a roughness sub-layer correction term. The assumption of a random arrangement of the roughness elements and their sheltering volumes, leads to express z_d by:

$$\frac{z_d}{h} = 1 - \frac{1 - \exp\left(-\sqrt{2C_{d1}\lambda_f}\right)}{\sqrt{2C_{d1}\lambda_f}}. \tag{2.19}$$

The system (18-19) is solved by computing $\frac{u_*}{U(h)}$, either by iteration of

$$\gamma = \frac{u_*}{U(h)} = \frac{\sqrt{C_{ds} + \frac{\lambda_f C_{dh}}{2}}}{\exp\left(\frac{c_w \lambda_f \gamma}{2}\right)}, \tag{2.20}$$

where c_w is a wake length parameter (related to the shear stress shelter area or momentum deficit sheltering volume of the roughness elements),

or from the simplified expression (*Raupach, 1994*):

$$\frac{u_*}{U(h)} = \min\left(\sqrt{C_{ds} + \frac{\lambda_f C_{dh}}{2}}, \left[\frac{u_*}{U(h)}\right]_{\max}\right), \tag{2.21}$$

where C_{ds} and C_{dh} are respectively the substrate surface and unit obstacle drag coefficients (estimated at level $z = h$). *Raupach (1994)* recommended: $C_{ds} = 0.003$, $C_{dh} = 0.6$, $\left[\frac{u_*}{U(h)}\right]_{\max} = 0.3$, $\Psi_{RSL} = 0.193$, and $C_{d1} = 7.5$. *Bottema & Mestayer (1998)* reported some imperfections in the model, and especially for very high densities where it cannot have a mathematical solution. Also, *Raupach (1995)* proposed some corrections to his models. Relations (20-21) can thus be replaced by:

$$\frac{u_*}{U(h)} = \sqrt{C_{ds} + \frac{1}{2}\lambda_f C_{dh}}, \quad \textit{with} \quad \lambda_f \le \lambda_{f,crit} = \frac{\frac{C_{dh}}{2} + \sqrt{\left(\frac{C_{dh}}{2}\right)^2 + 4C_{ds}\left(\frac{eC}{2}\right)^2}}{2\left(\frac{eC}{2}\right)^2}, \tag{2.22}$$

where: $e = 2.718$ and C is a model constant whose value may be within a range of 0.3-0.7.

In order to extend the *Lettau (1969)* model (see relation (7)) that was recognized to fail for the larger densities and that did not include z_d parameterizations, *Macdonald et al. (1998)* proposed a new model, summarized by *Grimmond & Oke (1999)* as the following:

$$\frac{z_d}{h} = 1 + \alpha^{\lambda_p}\left(\lambda_p - 1\right), \tag{2.23}$$

$$\frac{z_0}{h} = \left(1 - \frac{z_d}{h}\right)\exp\left(-\left(\frac{1}{2}\beta\frac{C_d}{\kappa^2}\left(1 - \frac{z_d}{h}\right)\lambda_f\right)^{-1/2}\right), \tag{2.24}$$

where: $C_d = 1.2$ is a drag coefficient, and α, β are empirical constants that must be adjusted to the building configuration. From an adjustment of this model with some wind tunnel data *Grimmond & Oke (1999)* recommended for staggered arrays of cubes: $\alpha = 4.43$ and $\beta = 1.0$.

As previously stated, the effective implementation of morphometric methods for a full city requires statistical analyses of urban databases containing both the land use descriptors and building geometric descriptors. Recently, such methods have been developed by *Bottema & Mestayer (1998)* (see also *Daniel & Hameon, 1996*) and *Ratti et al. (2000)* in urban digital elevation model software.

2.3. Assessment of Grimmond & Oke (1999) review

After *Bottema (1997)*, in order to test the morphometric models vs. experimental determinations of z_o and z_d, *Grimmond & Oke (1999)* reviewed more than 60 urban field studies and applied to experimental datasets the quality criteria of *Wieringa (1993)* and *Bottema (1997)*. This led them to retain only 9 datasets. In addition, only 14 scale model wind tunnel datasets were accepted. *Bottema (1997)* noted that a strict implementation of slightly more stringent quality criteria would have led them to reject virtually all datasets. Nevertheless, the accepted experimental data showed a considerable scatter, and especially for z_d with about half of estimations outside the envelope of the "reasonable limits". The scale model data did not improve the experimental evidence. Most of the wind tunnels are being too small to provide sufficiently developed surface layers over roughness elements of noticeable thickness. The considerable scatter in the experimental data do not allow to determine any "most probable" trends of z_0/h and z_d/h dependences to λ_f and λ_p. Nevertheless, *Grimmond & Oke (1999)* strongly favored models that incorporate λ_f, but they stressed also a need to incorporate other descriptors too. They especially noted the importance of building height variability, with a possible z_o linear increase with the standard deviation σ_h of roughness element heights. This influence of building height and roof variability was already observed by *Rafailidis (1997)* in a wind tunnel scale study and by *Guilloteau (1999)* in numerical simulations over periodic building arrays.

Tests of the models vs. individual datasets are (as expected) as disappointing as the experimental data themselves, showing poor performances. Nevertheless, *Grimmond & Oke (1999)* draw some conclusions of their comparisons essentially for the North American cities. Some of these conclusions have been already mentioned above for the "simple" morphometric models. As for more complex morphometric models, the complete model of Bottema for regular building arrays (relations 10-15) ranks first in general, followed by the random arrangement model of Raupach (relations 18-22), and the model of *Macdonald et al. (1998)* (relations 22-24). This ranking is proportional to the model demand in input requirements. These three models behave correctly in the complete range of λ_f and λ_p. The simplified model of Bottema (relations 10, 16, 17) scores nearly as well, and it can be applied also across the full range of λ_f and λ_p. Considering its relatively low input requirements, it is an efficient alternative. More simple models cannot be recommended, especially since their range of applicability is restricted. As for *Grimmond & Oke (1999)* "recommended rule of thumb", keeping in mind that it does not include any density dependency of z_o, it will therefore, overestimate z_o at the low and high densities, and underestimate it at the medium densities.

In addition, observing that many experimenters did not evaluate z_d, *Grimmond & Oke (1999)* stressed the importance of the z_d parameterization "in applications such as wind profile analysis, since it is the sum of $z_d + z_o$ that is required", this sum is being dominated by z_d. They also analyzed

the models for the blending height (level above which the inertial surface layer structure may be observed).

2.4. Morphologic methods

Considering the relatively poor performances of the present morphometric models, more empirical and pragmatic approaches can be considered, based on the visual observation of the physical structure of the urban canopy (e.g. for example, from aerial photography). From survey of experimental data, *Grimmond & Oke (1999)* offered a first-order evaluation of the roughness parameters of urban zones, separated only into 4 categories. These categories are associated with 4 flow regimes: (1) Low height and density – isolated flow; (2) Medium height and density – wake interference flow; (3) Tall and high density – skimming flow; (4) High rise – chaotic or mixed flow.

Ellefsen (1990, 1991) designed a scheme to identify 17 types of urban terrain zones that are defined by a written description and model photography. Furthermore, *Grimmond & Oke (1999)* adapted this scheme to the proposed 4 urban roughness categories, offering physical description, matrix of typical photographs, and table of the most probable non-dimensional roughness parameters. In addition to these pragmatic approaches, we must further note the revision of the classical Davenport classification of effective terrain roughness, which included explicitly the urban terrains (*Davenport et al., 2000*) (Tab. 2.4.1).

z_o (m)	Landscape description	Comment
1: 0.0002 *"Sea"*	Open sea or lake (irrespective of wave size), tidal flat, snow-covered flat plain, featureless desert, tarmac and concrete, with a free fetch of several kilometers.	
2: 0.005 *"Smooth"*	Featureless land surface without any noticeable obstacles and with negligible vegetation; e.g. beaches, pack ice without large ridges, marsh, and snow-covered or fallow open country.	
3: 0.03 *"Open"*	Level country with low vegetation (e.g. grass) and isolated obstacles with separations of at least 50 obstacle heights; e.g. grazing land without windbreaks, heather, moor and tundra, runway area of airports. Ice with ridges across-wind.	
4: 0.10 *"Roughly open"*	Cultivated or natural area with low crops or plant covers, or moderately open country with occasional obstacles (e.g. low hedges, isolated low buildings or trees) at relative horizontal instances of at least 20 obstacle heights.	
5: 0.25 *"Rough"*	Cultivated or natural area with high crops or crops of varying height, and scattered obstacles at relative distances of 12 to 15 obstacle heights for porous objects (e.g. shelterbelts) or 8 to 12 obstacle heights for low solid objects (e.g. buildings).	*Analysis may need z_d*
6: 0.5 *"Very rough"*	Intensively cultivated landscape with many rather large obstacle groups (large farms, clumps of forest) separated by open spaces of about 8 obstacle heights. Low densely-planted major vegetation - bush-land, orchards, young forest; area moderately covered by low buildings with inter-spaces of 3-7 building heights and no high trees.	*Analysis requires z_d*
7: 1.0 *"Skimming"*	Landscape regularly covered with similar-size large obstacles, with open spaces of the same order of magnitude as obstacle heights; e.g. mature regular forests, densely built-up area without much building height variation.	*Analysis requires z_d*
8: *2 "Chaotic"*	City centers with mixture of low-rise and high-rise buildings, or large forests of irregular height with many clearings.	*Analysis by wind tunnel advised*

Tab. 2.4.1. Revised Davenport classification of effective terrain roughness, including urban terrains (*Davenport et al., 2000*).

2.5. Urban database analysis for mapping morphology and aerodynamic parameters: St. Jerome case study, ESCOMPTE

It is well known that the presence of city will modify surface properties and local meteorology. Therefore, for numerical high-resolution simulation with soil and atmospheric models, it is important to know the city structure and its components. The study area of 4 x 4 km (St. Jerome study area, city of Marseille, France) was selected as a specific case of an urban area composed of several types: collective, individual, and sparse buildings; vegetation; water surfaces; etc. (Fig. 2.5.1).

Fig. 2.5.1. The St. Jerome study area [buildings ( ), vegetation ( ), road network (one lane: , two lanes: , three lanes: , four lanes: ◊) and water surface].

The urban topographic database BDTopo (French National Geographic Institute, IGN) was used to analyze an urban structure of Marseille in order to characterize the morphology of settlements and land coverage (*Long et al., 2002*). First, since the database was built on aerial photographs of 1994, an analysis of its representativeness vs. ground reality was performed by comparison with maps of IGN (1:25000, 1999), SPOT-4 satellite images (15 m resolution), and U-GIS data of Marseille (*Long et al., 2003a*). This allowed to introduce corrections for surfaces of cover modes. Second, the accuracy of the computed descriptive statistics was estimated for different sizes of grid cells. It was found that the individual cells of 200 x 200 m (i.e. 4 ha) represent best the structure of each urban district with respect to both high resolution and statistical representativeness (*Long, 2003c*). Therefore, for this size cells mean variables describing the buildings morphology and land covers were computed onto a grid and composed a GIS : building average height, perimeter, volume, compactness, plan area density, vegetation and pavement densities, etc. Moreover, aerodynamic parameters such as roughness length and displacement height were estimated.

For the St. Jerome study area (*Long et al., 2003b; Long, 2003c*), it was found that an average height of buildings is 7.7 m with 50% of these buildings having heights within a range of 4.8-9.7 m. Many buildings are small because, on average, the perimeter and volume are 62.5 m and 3192 m^3, respectively. The maximum volume is 98514 m^3 with 50% of buildings having volumes within a

range of 620-3277 m^3. The pavement density is 0.08. The building and vegetation densities - 0.10 and 0.09, respectively - differed by only 10%. Moreover (as shown in Fig. 2.5.2), in the northern part of the St. Jerome study area, the building densities and heights are lower compared with the southern part. The histograms show that both building height and density are skewed with maxima corresponding to cells in the southern part and an extreme on border between the urban and rural areas in the northern part (cf. Fig. 2.5.1).

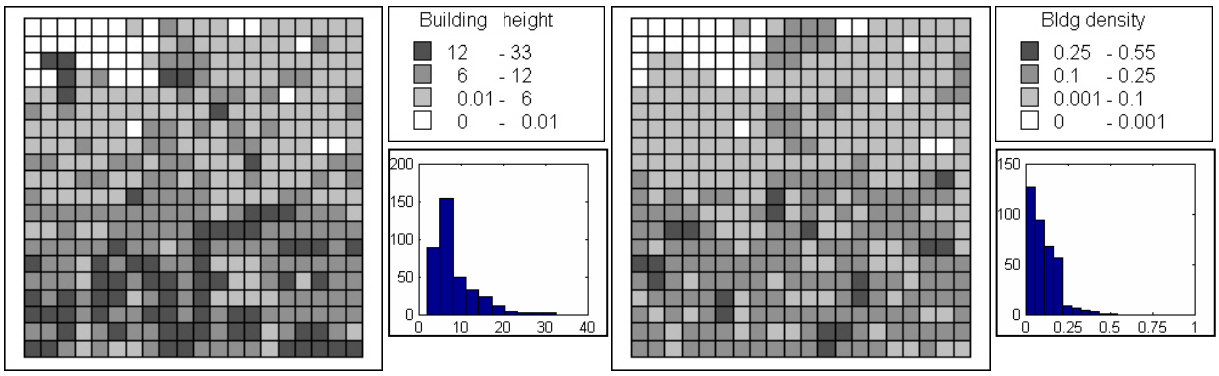

Fig. 2.5.2. Average building height (left) and building plan area density (right) for the St. Jerome district (each shown grid cell has a resolution of 200 x 200 m).

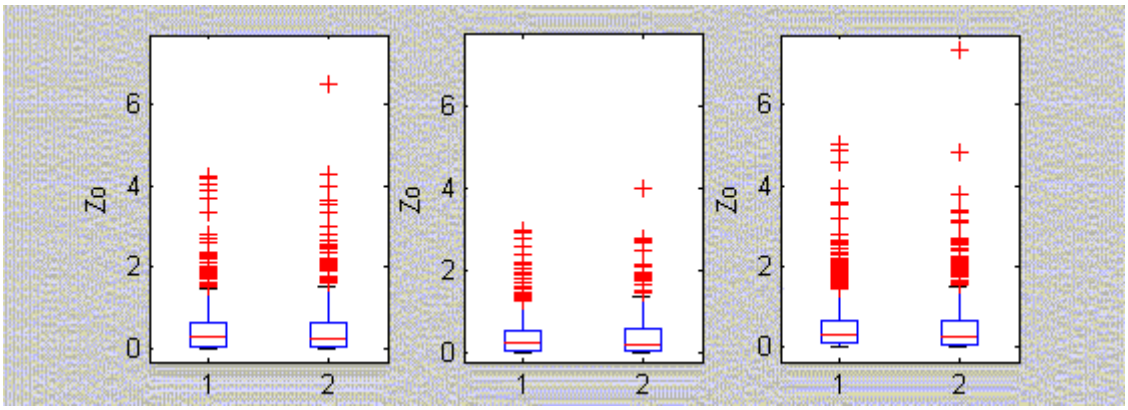

Fig. 2.5.3. Roughness length obtained based on models of Bottema (left), Raupach (middle), and Macdonald (right) for the St. Jerome study area for the north (1) and west (2) wind directions.

Three models (*Raupach, 1994; Bottema, 1995; Mcdonald et al., 1998*) were used to estimate a roughness length z_0 (in m) based on the building plan arrangement, plan and frontal densities of buildings. The distributions (shown as box-plots) of the roughness values ($z_{0(B)}$ - Bottema, $z_{0(R)}$ - Raupach, and $z_{0(M)}$ – Macdonald models) for each model for two selected wind directions - north and west - are shown in Fig. 2.5.3. The difference between z_0 is relatively low, but there is an extreme value for the west wind direction. The average $z_{0(R)}$ of 0.44 is noticeably lower compared with the average z_{0B} of 0.52 and z_{0M} of 0.56. It should be noted that 50% of $z_{0(B)}$ and $z_{0(M)}$ values are contained within a wider range of 0.06/0.09-0.63 compared with $z_{0(R)}$ (0.08-0.57). The standard deviation is higher and this underlines a non-homogeneity of the urban area. Moreover, the higher values of z_0 are observed in the southern part of the St. Jerome study area, where buildings are taller as well as the building plan area density is higher.

3. Improved models for urban roughness sublayer simulation

For urban areas the Monin-Obukhov (MO) similarity theory does not work satisfactory inside the urban canopy. So, the classical theory with a corrected calculation of the urban roughness, as it was considered in the previous chapter, does not give a complete solution for the NWP model urbanisation. Therefore, it is necessary to further develop the parameterisations of the urban roughness sublayer to make it suitable for meteorological models.

One of the most common way to avoid or minimise this problem is to consider the MO theory profiles in the models from an elevated level of the displacement height. Therefore for urban areas the roughness should be characterised by, at least, two parameters: the roughness length, z_0, and the displacement height, z_d. Theoretical aspects of such approach realisations were discussed by *Belcher et al.* (2003), *Hunt et al.* (2003), *Zilitinkevich et al.* (2003), *Rotach et al*. (2002) and in several reports of the COST Action 715 (*COST, 2001, 2002*). In this report we will focus on some further developments of the roughness effect parameterisations for urban areas in connection to their possible implementation in urban-scale NWP models.

3.1. Effective roughness and flux aggregation technique

by Alexander Baklanov (DMI)

In a general manner, the roughness length is considered on the assumption that the surface is relatively homogeneous and can be characterised by a value of z_0. Over urban areas, the atmospheric boundary layer is strongly influenced by the roughness heterogeneity of urban quarters patchwork, especially at the city boundaries. In numerical simulations the vertical momentum transfer is most commonly parameterised by a grid-cell averaged roughness length, while the urban roughness lengths may vary by several orders of magnitude. Therefore, it is not enough to calculate the roughness parameters for the urban areas according to the methods considered in Ch. 2, and rather consider the concept of an effective roughness to treat urban areas in NWP and meso-meteorological models. There are several publications introducing and testing the effective roughness for different types of heterogenic terrains, e.g., for forest-grass canopies, land-sea interaction, etc. (*Taylor, 1987; Gutman et al., 1998; Hasager et al., 2003; De Rider, 2003; Schlunzen and Katzfey, 2003*).

The influence of strong roughness changes on the neutrally stratified atmospheric boundary layer simulation was explored by *Mestayer et al. (2003)* in two parts, with a view of optimizing the geographical representation of the aerodynamic characteristics of urban quarters in high resolution numerical simulations using an advance 3D atmospheric model. In this first part, the influence of isolated, strong transitions are assessed for 2D and 3D geometries. First, the structure of the developing internal boundary layer (IBL) after an isolated roughness step was explored showing that a new constant flux layer extends only about one tenth of the IBL height inducing a strong momentum variation in the transition layer above with this momentum excess still noticeable several kilometres downstream from the step. Roughness strips are seen to influence largely more the turbulent fields than the mean wind field and their perturbations extend over several kilometres downstream and a few tens of metres upwards. The perturbations generated by the transitions themselves, through the pressure field equilibrium loss, are larger by a factor of 2-3 than if the equilibrium with the new roughness was reached immediately. The perturbations generated by 3D spots are less intense than by the corresponding 2D strips, and they do not much extend in the lateral direction, but neighbouring island perturbations may nevertheless reinforce each other. This study gives a nice possibility to study the effective roughness with a high resolution, but it is quite expensive for NWP models.

So, it is reasonable to simulate the effective roughness fields for a considered city separately for different situations (e.g., for different seasons, wind directions) and to build a kind of effective roughness maps library. For such strategy, a new flux aggregation technique suggested by Risø National Laboratory in cooperation with DMI (*Hasager et al., 2002, 2003*), was installed in the DMI-HIRLAM model but only for non-urban areas for the moment.

Fig. 3.1.1 gives a schematic structure of the surface flux microscale aggregation model (the left figure – a simple version "H" according to *Hasager & Jensen (1999),* the right figure – a more advance version "z0t", according to *Hasager et al. (2002)*).

A short description of the algorithm is the following. The inputs are wind speed (*U*), air temperature (*Ta*) at the computational level and maps of surface temperature, land cover classes and leaf area index (LAI) from satellite. The aerodynamic roughness map (z_0) is generated from the index list except for water bodies. The index number and an equation for the scalar roughness z_{0t} are prescribed for each land cover type to provide the z_{0t} map. The model runs within the dotted red line. The atmospheric flow equations are linearised and solved by Fast Fourier Transform (FFT). The output maps are the friction velocity (u_*), the temperature scalar (θ_*), the roughness map (z_0) and the scalar roughness map (z_{0t}) all of which are found through iteration (indicated by the green curved arrows). The iteration is due to the stability function. The final output is a map of the sensible flux (*H*).

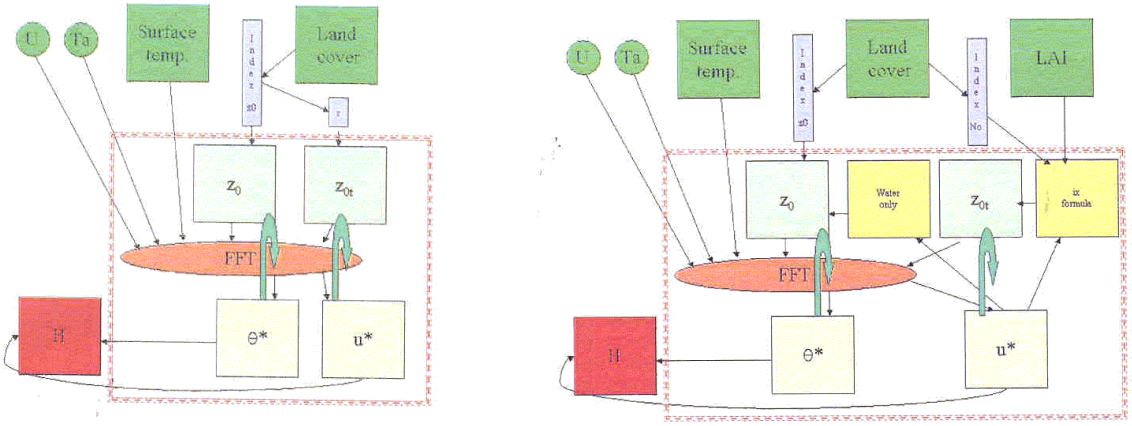

Fig 3.1.1. New flux aggregation technique suggested by Risø NL in cooperation with DMI (*Hasager et al., 2002*): version "H" (left) and version "z0t" (right).

Using fields of effective roughness length, satellite-based sea surface temperature and albedo in DMI-HIRLAM-E model would give the possibility to treat the urban area non-homogeneities with more detail structure and specific effects. It is planned to extend the above approach to the urban canopies as well. However, we need experimental data to verify the parameterisations for urban areas and to check the applicability of the linear approximation in the model for urban conditions.

3.2. Effect of stratification on the surface resistance over very rough surfaces

by Sergej Zilitinkevich, Alexander Baklanov and Sylvain Joffre

NWP and meso-meteorological models consider the roughness length, z_0, as a constant for each grid cell with different combinations of land-use classes, according to classical theory. However, based on experimental data, several authors showed that z_0 may depend on the temperature stratification (*Arya, 1975*; *Joffre, 1982; Wood and Mason, 1991; Hasager et al., 2002)*. Especially, this effect can be considerable for very rough surfaces, like the urban canopy. However, there were no theoretical background and practical parameterizations for the dependences z_0 on the atmospheric stability. Let us consider separately the roughness length, z_0, for stable and unstable stratifications.

3.2.1. Stable stratification

Consider the familiar velocity-gradient formulation for the stable stratification:

$$\frac{du}{dz} = \frac{u_*}{\kappa z}\left(1 + C_u \frac{z}{L}\right) \approx \begin{cases} \dfrac{u_*}{\kappa z} & \text{at } z < z_{**} \equiv \dfrac{L}{C_u} \\ \dfrac{C_u u_*}{\kappa L} & \text{at } z > z_{**}, \end{cases} \tag{3.1}$$

where $C_u \approx 2.1$ (Høgstrøm, 1995; latest studies (e.g., Esau, 2003) show that the value of C_u is higher, ≈ 2.8) is an empirical dimensionless constant, z_{**} is a matching height, and L is the Monin-Obukhov length:

$$L = \frac{-u_*^3}{F_{bs}}, \tag{3.2}$$

Where $F_{bs} = \beta F_{\theta s} + 0.61 g F_{qs}$ is the buoyancy flux at the surface, which includes the temperature flux, $F_{\theta s}$, and the humidity flux, F_{qs}; F_{qs}; g is the acceleration due to gravity; $\beta = g / T_0$ is the buoyancy parameter; and T_0 is a reference value of absolute temperature.

Eq. (1) yields to the following eddy viscosity profile:

$$K_M = \frac{u_*^2}{du/dz} = \begin{cases} \kappa u_* z & when \quad z > z_{**} \\ \kappa u_* z_{**} & when \quad z = z_{**} \end{cases} \tag{3.3}$$

and wind velocity profile:

$$u = \frac{u_*}{\kappa}\left(\ln\frac{z}{z_{0u}} + C_u \frac{z}{L}\right) \approx \begin{cases} \dfrac{u_*}{\kappa}\ln\dfrac{z}{z_{0u}} & \text{at } z < z_{**} \equiv \dfrac{L}{C_u} \\ \dfrac{u_*}{\kappa}\ln\dfrac{z_{**}}{z_{0u}} + \dfrac{C_u u_*}{\kappa}\dfrac{z - z_{**}}{L} & \text{at } z > z_{**}, \end{cases} \tag{3.4}$$

where z_{0u} is the roughness length for momentum For reasonably rough land surfaces z_{0u} is 10 to 30 times smaller than the characteristic height of the roughness elements, h_0 (e.g., *Monin & Yaglom, 1971*). For a big city, $h_0 \approx 30$ m.

Recall that stable stability conditions with the MO length $L \approx 50$ m or less is not exceptional. In the case that

$$L < C_u h_0 = (10 \div 30) C_u z_{0u},$$

the logarithmic interval in the velocity profile does not exist, and the near-surface flow acquires some properties of the laminar flow:

- The eddy viscosity becomes depth-constant: $K_M \sim \frac{\kappa}{C_u} u_* L$.
- The wind profile becomes linear, $u(z) = \frac{C_u u_* z}{\kappa L}$, and insensitive to the presence of roughness elements. Physically this means that hollows between roughness elements are filled with so dense fluid that the surface becomes as if dynamically smooth.

To include this regime in the context of the traditional parameterization of the flow-surface interaction, consider a "quasi-viscous sub-layer" depth scale analogous to the usual viscous sub-layer depth $\delta = \nu / u_*$, where ν is the molecular viscosity. Substituting our depth-constant eddy viscosity $K_M \sim \kappa C_u^{-1} u_* L$ for ν, yields

$$\delta_* = \frac{K_M}{u_*} = \kappa C_u^{-1} L . \tag{3.5}$$

Now recall that for dynamically smooth surfaces the effective roughness length is $z_{0u} = 0.1\delta$ (e.g. *Monin & Yaglom, 1971*). Hence in sufficiently stable stratification [determined by Eq. (3.4)] the roughness length becomes

$$z_{0u} = 0.1\delta_* = 0.1\,\kappa C_u^{-1} L \approx 0.02L. \tag{3.6}$$

Then a reasonable interpolation formula for the effective roughness length covering neutral, moderately stable and very stable stratification regimes is

$$\frac{1}{z_{0u-effective}} = \frac{1}{z_{0u}} + \frac{C_{0S}}{L}, \quad \text{which yields} \quad z_{0u-effective} = \frac{z_{0u}}{1 + C_{0S} z_{0u} / L} . \tag{3.7}$$

Here, C_{0S} is an empirical dimensionless constant. The above analysis suggests its reference value: $C_{0S} = 10 C_u \kappa^{-1} \approx 50$.

To include regimes over very smooth surfaces (such as ice or snow) consider the classical viscous sub-layer limit:

$$\frac{1}{z_{0u-effective}} = \frac{1}{z_{0u}} + \frac{10 u_*}{\nu}, \tag{3.8}$$

Then instead of Eq. (3.7) a more general interpolation formula could be proposed:

$$\frac{1}{z_{0u-effective}} = \frac{1}{z_{0u}} + \frac{C_{0S}}{L} + \frac{C_{0\nu} u_*}{\nu}, \quad \text{which yields} \quad z_{0u-effective} = \frac{z_{0u}}{1 + C_{0S} z_{0u} / L + C_{0\nu} z_{0u} u_* / \nu}, \tag{3.9}$$

where $C_{0\nu} \approx 10$ is a dimensional constant.

Notice that Eq. (3.9) includes a well-known simplified version: $z_{0u-effective} / z_{0u} = (1 + C_{0\nu}\,\mathrm{Re})^{-1}$, where $\mathrm{Re} = z_{0u} u_* / \nu$ is the surface Reynolds number. This formula reasonably accurately describes the transition between the smooth and the rough surface regimes.

3.2.2. Unstable stratification

The velocity profile in unstable stratification is given by (e.g., *Kader & Yaglom, 1990*):

$$\frac{du}{dz} = \begin{cases} \dfrac{u_*}{\kappa z} \text{ at } z_{0u} << z < z_* \equiv C_* \mid L \mid \\ \dfrac{C_U u_*^2}{F_{bs}^{1/3} z^{4/3}} \text{ at } z > z_*, \end{cases} \tag{3.10}$$

$$u = \begin{cases} \dfrac{u_*}{\kappa} \ln \dfrac{z}{z_{0u}} \text{ at } z_{0u} << z < z_* \\ \dfrac{u_*}{\kappa} \ln \dfrac{z_*}{z_{0u}} + \dfrac{3 C_U u_*^2}{F_{bs}^{1/3}} \left(z_*^{-1/3} - z^{-1/3} \right) \text{at } z > z_*, \end{cases}$$

where $C_U \approx 1.7$ is an empirical constant. When $|L|$ is very small or the height of the roughness elements, h_0, very large so that $h_o > C_* \mid L \mid$, there is no room for the log profile. Then the free-convection form of the velocity gradient extends down to the roughness layer:

$$\frac{\partial u}{\partial z} = \frac{C_U u_*^2}{F_{bs}^{1/3} z^{4/3}}. \tag{3.11}$$

In this regime the turbulence of purely convective origin dominates throughout the surface layer and controls the flow-obstacle interaction. Accordingly the velocity profile cannot be described by the two-layer "mechanical + convective turbulence" model, Eq. (3.10), which involves the traditional roughness length.

Clearly, the free convection formulation for the eddy viscosity, $K_M = C_U^{-1} F_{bs}^{1/3} z^{4/3}$ [consistent with Eq. (3.11)], becomes inapplicable in the roughness layer, where the turbulent length scale is no longer proportional to the distance from the surface, z. Instead it could be taken proportional to the typical height of the roughness elements, $h_0 \sim 30 z_{0u}$. Because the energy production is basically due to the buoyancy forces, a reasonable scaling estimate of the eddy viscosity in the roughness layer becomes $K_M \sim F_{bs}^{1/3} (30 z_{0u})^{4/3}$.

Interpolating between the above two formulae for K_M, namely, taking

$$K_M = C_U^{-1} F_{bs}^{1/3} (z + C_0 z_{0u})^{4/3} \tag{3.12}$$

gives the mean velocity profile:

$$u(z) = \frac{3 C_U u_*^2}{F_{bs}^{1/3}} \left[\frac{1}{(C_0 z_{0u})^{1/3}} - \frac{1}{z^{1/3}} \right], \tag{3.13}$$

where C_0 is a dimensionless constant. *Grachev et al. (1997)* compared Eq. (3.13) with observational data and concluded that the "free-convection roughness length", $C_0 z_{0u}$, is essentially larger than the usual roughness length z_{0u}. This looks physically reasonable. Indeed, in strong convection the buoyancy driven eddies in the roughness layer penetrate down to the very bottom of the hollows between the roughness elements, which is why the turbulent length scale could be as large as the total height of the roughness elements $h_0 \sim 30 z_{0u}$.

It is conceivable that even before achieving the free convection regime in the roughness layer,

the role of the buoyancy forces in this layer could be pronounced. Then, in the light of the above reasoning, the effective roughness length $z_{0u-effective}$ should increase with increasing $z_{0u}/|L|$ from the neutral-stability value z_{0u} towards the free-convection value $C_0 z_{0u}$.

The dependence of $z_{0u-effective}/z_{0u}$ on $z_{0u}/|L|$ should be determined empirically. Analytical approximation of this dependence is not a principal issue. For example, it could be taken

$$\frac{z_{0u-effective}}{z_{0u}} = \left[C_0 - (C_0 - 1)\exp(-C_1 z_{0u}/|L|)\right], \text{ or} \tag{3.14}$$

$$\frac{z_{0u-effective}}{z_{0u}} = \left[\frac{1}{1 + z_{0u}/|L|} + C_0 \frac{z_{0u}/|L|}{C_1 + z_{0u}/|L|}\right], \tag{3.14a}$$

where C_1 is an empirical constant, or any other way – as dictated by experimental data.

3.2.3 Comparison between theory and empirical evidence

The expressions developed above for the dependence of z_0 against buoyancy forces imply that z_0 decreases as stability increases for rough surfaces. Under unstable cases, (3.14) is more difficult to interpret and depend on the numerical value of the unknown constants C1 and C2, but an increase of zo is expected from physical reasoning.

From accurate wind tunnel data over a smooth surface, Arya (1975) found that the depth of the viscous layer increases while the skin friction decreases with increasing stability, implying a decrease of the roughness. Joffre (1982), also observed a sharp decrease of the roughness parameter z_o with increasing stability, for a ice-covered sea surface (conditions going from smooth to slightly rough). On the other hand, both authors did not find any clear trend under unstable cases, except for a slim indication of an increase of z_o under their most unstable conditions.

Both authors explained their observations by the fact that possibly the stabilising effect of buoyancy suppresses turbulence more effectively than viscosity alone would do. Joffre (1982) proposed an expression for the thickness of the viscous sub-layer which displays an increase under stable conditions but a slower decrease under unstable conditions. In other words, work done against the force of gravity neutralizes turbulence production by the mean flow and an increasing buoyancy flux leads to a thickening of the viscous sub-layer, an increase in the profile constant representing the intercept with the z_0-level and a reduction in the roughness length z_0. Joffre (1982) also the envisaged the possibility that this observed z_0-dependence may be an artefact of a missing correction to be made to the MO-theory due to the coupling between radiative and turbulence flux which should modify the theoretical profiles.

3.3. Roughness for momentum, heat, and moisture

by Alexander Baklanov (DMI)

The determination of the turbulent fluxes of momentum, heat and moisture in NWP models by way of bulk transfer equations requires the specification of the aerodynamic roughness length (for momentum), z_0, and the scalar roughness lengths: for temperature, z_{0t}, and for moisture, z_{0q}. Most of the NWP and meso-meteorological models for surface layer profiles consider the scalar roughness lengths, z_{0t} and z_{0q}, equal to the roughness for momentum, z_0. However, numerous experimental

data (*Garratt, 1992; Mahrt & Ek, 1993; Mödler & Lindroth, 1999*) show that, especially for very rough surfaces such as urban canopies and forests, this approximation can lead to quite erroneous results for the heat and moisture fluxes. Measurements indicate values for $kB^{-1} \equiv \ln(z_0/z_{0t})$ (*Garratt, 1992*) of about 2 for natural vegetation and up to 20 and more for urban surfaces.

Theoretical studies (*Zilitinkevich, 1970; Brutsaert, 1975; Jensen et al., 2002*) suggest that the ratio z_{0t}/z_0 is a function of the roughness Reynolds number $Re_* = (u_* z_0)/\nu$, where ν is the kinematic viscosity. However, in general this ratio is relevant mostly for moderately rough surfaces and was not verified for urban conditions.

In the flux aggregation technique, mentioned in Chapter 3.1, according to (*Hasager et al., 2002*), the following equation for z_{0t} is suggested for use in the case of a rough surface (including urban areas):

$$z_{0t} = \frac{z_0}{\exp\left(23.1\sqrt{u_*}\right)}. \tag{3.15}$$

However, it is necessary to mention that the above formulation was not verified for urban conditions versus city area measurement datasets.

Recently Voogt and Grimmond (2000) studied the sensible heat fluxes over a light industrial area in Vancouver, British Columbia, Canada from observed tower fluxes and modelled using a bulk heat transfer approach. Sensitivity analyses of the various surface temperature estimates were performed. Estimates of the ratio of roughness length of momentum to heat, κB^{-1}, for this area were in general agreement with theoretical estimates for bluff-rough surfaces and are larger than those documented for vegetated and agricultural surfaces. Back-calculated values do vary depending on the method used to determine surface temperature but vary more with the time of day. Empirical relations derived previously for vegetated surfaces were shown to agree well with the results for a dry urban environment, but approaches based on micro-scale variability in temperature fields were problematic. So, following previous studies of *Brutsaert (1982)* and *Brutsaert and Sugita (1996)*, they suggested using the following formulation for z_{0t} for bluff-rough situations:

$$z_{0t} = z_0\left[7.4\exp(-2.46\,\mathrm{Re}_*^{0.25})\right], \tag{3.16}$$

with Re_* is the roughness Reynolds number as was introduced above.

In relation to the Brutsaert-model for κB^{-1}, Joffre (1988) modified one fluid dynamics assumption of Brutsaert concerning the level under which the log-profile is not valid by using the Reichardt's profile that has the merit to cover the full structure from the surface through the transitional layer up to the log-layer above. This yields a modification of one numerical constant in the Brutsaert's model, after what the new formula perfectly fits the compilation of observations of Garratt and Hicks (1973) for various bluff types of roughness over a wide range of the roughness Reynolds number ($0.1 \le Re_* \le 100$). This modification yields

$$z_{0t} = z_0\left[20\exp(-7.3\kappa a_c\,\mathrm{Re}_*^{0.25}\,Sc^{1/2})\right], \qquad \text{for } Re_* > 0.15 \tag{3.17}$$

where a_C is the inverse turbulent Schmidt number (= K_H/K_M for z_{0t} or K_E/K_M for z_{0q}) and Sc the Schmidt number ($=\nu/D_C$, D_C is the molecular diffusivity of the particular property, i.e., heat, moisture but also gaseous compounds). The original Brutsaert's formula had a coefficient 7.4

instead of 20 in the first term of the right-hand side and was valid for $Re_*>2$ (rough case only). Equation (3.17) matches the corresponding expression (3.18) valid for aerodynamically smooth case at $Re_*=0.15$, i.e.:

$$z_{0t} = 30(\nu / u^*)\exp\left[-13.6\,\kappa\, a_c\, Sc^{2/3}\right] \qquad \text{for } Re_*<0.15\,. \tag{3.18}$$

Taking the parameters mentioned above into account, a series of sensitivity studies was performed by *De Rider* (2003) using the Advanced Regional Prediction System (ARPS) to evaluate their impact on the urban surface energy balance. It was found that albedo and emissivity, which both act on the radiation balance, have a relatively small impact within their respective range of values. Indeed, there is a rather small difference between the urban and rural radiation balances, as the increased loss of net thermal long-wave radiation for cities is partly compensated for by a gain in net shortwave radiation due to a lower albedo. Moisture availability is an important parameter, as it affects the partitioning of incoming radiant energy between the turbulent fluxes of sensible and latent heat. The impermeability of urban surfaces generally reduces the availability of soil moisture for evaporation, thus leading to low latent heat flux values in cities. In order to account for this phenomenon, the land-surface scheme was adapted by inhibiting the infiltration of precipitation for the non-vegetated portion of urban land use types. As a main conclusion of this parameter analysis, it was found that the main cause of the observed high values for the heat storage flux resides in the large ratio of the roughness length for momentum versus heat characterising cities. The reason is relatively straightforward: on the one hand, momentum roughness is high, resulting in comparatively low wind speeds close to the urban surface. On the other hand, these low wind speeds, combined with the extremely low values for the heat roughness, result in a very high resistance for turbulent heat fluxes, thus strongly inhibiting the latter. Not only does this explain the large ratios of storage versus sensible heat, it is also consistent with the observed high urban surface temperatures.

So, concluding this chapter, we have to stress the importance of the separate simulations of the aerodynamic roughness length, z_0, and the scalar roughness lengths: for temperature, z_{0t}, and for moisture, z_{0q}, in city-scale NWP models. Some available parameterisations for the scalar roughness length in the urban areas are suggested here for practical testing in NWP models of the FUMAPEX partners, however this problem needs further studies and verifications.

3.4. Urban roughness layer exchange parameterisation

by Alain Clappier (EPFL)

The classical technique used to simulate the effects of the earth surface in mesoscale models is based on constant-flux layer approximation in the surface layer (Monin-Obukhov Similarity Theory or MOST). However, measurements over different cities in the world (Zuerich - *Rotach, 1993*, Sapporo - *Oikawa & Meng, 1995*, and Vancouver - *Roth & Oke, 1993*) as well as wind tunnel studies (*Kastner-Klein et al., 2001*) have shown that turbulent fluxes are height dependent in the urban canopy. This means that MOST can not be applied in the so-called Urban Roughness Sublayer, URS (from street level up to 50-100 m). Instead, *Rotach (2001)* suggested adapting a local scaling approach in this layer.

Two main approaches exist to simulate the effect of the urban canopy:

- One (*Bottema, 1997*) consists in modifying the MOST approach by finding a proper value for the roughness length, starting from urban characteristics (e.g. building density, building height) and the atmospheric stability (Monin-Obukhov length). In this case, the lowest model level is close to the top of the urban canopy (displacement height) because the MOST profiles are not valid below that level. Consequently, even if this method takes into account the effect of the urban canopy it does not provide any results inside the Urban Roughness Sublayer which is a critical region where pollutants are emitted and where people live.
- Alternatively, in another approach source and sink terms are added in the momentum, energy and turbulent kinetic energy equation to take into account the buildings. Different parameterizations (*Masson, 2000; Kusaka et al., 2001; Martilli et al., 2002*) had been developed to estimate the radiation balance (shading and trapping effect of the buildings), the heat, the momentum and the turbulent fluxes inside the urban canopy, taking into account a simple geometry of buildings and streets (three surface types: roof, wall and road).

During BUBBLE (Basel UrBan Boundary Layer Experiment), the exchange processes near the urban surface, as well as the flow in the upper part of the Urban Boundary Layer (UBL) have been investigated using surface and remote sensing instrumentation in the city of Basel (Switzerland). The measurements are taken from the main urban surface site "Basel-Sperrstrasse", located in a heavily built-up part of the city (”European urban”, dense urban, mainly residential 3 to 4 store buildings in blocks, flat commercial and light industrial buildings in the backyards). The measurement setup consists of a tower inside a street canyon reaching up to 32 m (2.2*h*), where the flow and turbulence field as well as energy fluxes were measured. The experimental surface tower was operated approximately one year. The instrumentation was heavily extended during the IOP between 15 June 2002 and 12 July 2002.

In order to study the meteorology inside and above the street canyon, the detailed urban parameterization scheme of *Martilli et al. (2002)* was implemented in a mesoscale model. The model was run off-line on a vertical column (1D), using measurements from a tower (30 m above ground level) for the upper boundary conditions, and calculated vertical profile for several meteorological parameters in the street canyon (Fig. 3.4.1). The validation of the model is made with measurements from the tower in the street canyon and directly above the urban canopy.

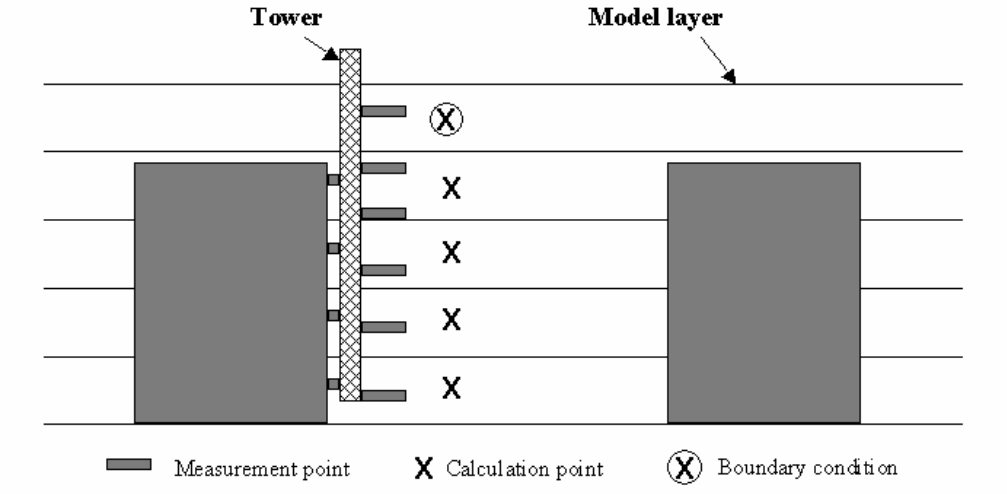

Fig 3.4.1. The configuration of 1D off-line model, with forcing at the top of the tower, and calculation from this point down to the ground in the street canyon.

The results (Fig. 3.4.2) show that the urban parameterization scheme is able to catch most of the typical processes induced by an urban surface: Inside the canopy layer, the wind speed, the friction velocity and the atmospheric stability are reduced. On the other hand, even if the main effects of the urban canopy are reproduced, comparison with measurements seem to indicates that some physical processes are still missing in the parameterization. In most of the cases, the model still overestimates the wind speed inside the canopy layer and it can have difficulties to simulate the maximum of the friction velocity which appears above the building roofs.

The wind speed and turbulence inside the urban canopy have a direct impact on the concentrations of primary pollutants which are emitted in the streets. For this reason, the improvement of the urban parameterization is one of the key point for the accuracy of primary pollutant forecasting.

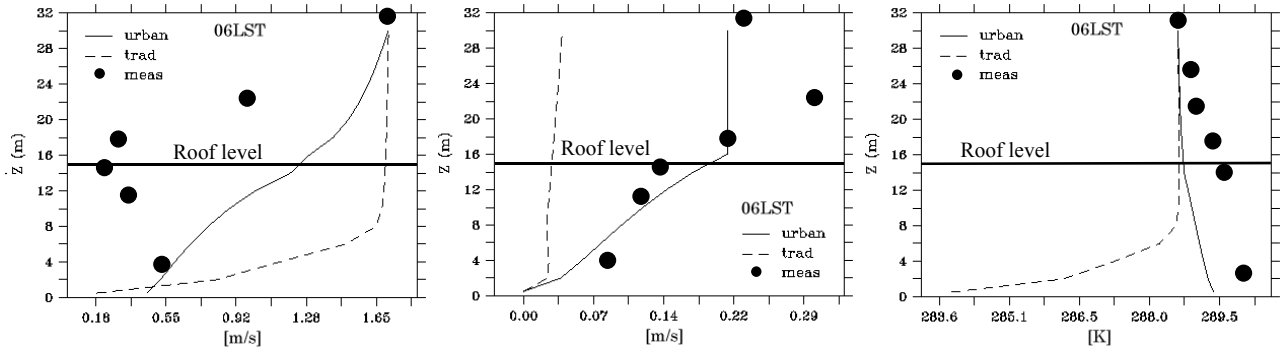

Fig 3.4.2. Vertical profiles of wind velocity (left), friction velocity (middle), and potential temperature (right) measured (points), simulated with MOST (dashed line) and with the urban parameterization of *Martilli et al. (2002)* (solid line).

4. Experimental study of urban roughness inhomogeneity effects on the UBL development

by Merike Schultz, Bernd Leitl, Michael Schatzmann (MIHU)

4.1. Motivation

Operational NWP models and meso-scale models in general work with horizontal resolutions of several km. This resolution is too coarse to resolve buildings and other obstructions. Obstacles that shape the urban canopy can only be taken into account by mean of a roughness parameterisation. Since the flow in the lowest (about) 100 m above ground is strongly affected by the obstacles, the quality of predictions obtained with ”urbanized” meso-scale models depends crucially on the quality of the urban roughness parameterisation these models apply.

It is common practice in numerical modelling to adjust the roughness characteristics from grid cell to grid cell whereas within one individual grid cell, which can cover several square km, the roughness properties are assumed to be everywhere the same. Although the values chosen might be a representative average for the grid cell as a whole, locally large deviations from the average must be expected since the roughness structure in real urban sites is typically non-uniform.

Basic questions of the following kind arise: Which fetch is needed behind a roughness change until a boundary layer flow regains equilibrium with its underlying surface?. Is the fetch needed the same for mean and turbulent properties or do turbulent properties have a longer ”memory”? Which velocity and flux profiles are characteristic for the equilibrium layer above the buildings? At MIHU (Meteorological Institute at Hamburg University), scientists have tried to provide answers to these questions by carrying out a few well-defined wind tunnel experiments with uniform cube roughness elements.

4.2. Basic definitions

After a step change of roughness the flow needs some time until it adjusts to the new underlying surface and until it reaches a new equilibrium. The height over which the ground roughness affects the flow increases with fetch (= distance from the roughness step). Fig. 4.2.1 shows a conceptual sketch of the flow development.

The roughness parameterisation used in mesoscale models covers typically the lowest few decametres of the boundary layer. It is presently common to assume here the existence of a logarithmic mean velocity profile and a constant momentum flux $\overline{u'w'}$. Both are characteristic features of the inertial sublayer. Fig. 4.2.1 indicates that directly behind a roughness step an inertial sublayer does not exist at all. Only after several roughness heights, an inertial sublayer starts to grow above the roughness layer. The fetch needed until the boundary layer attains a new equilibrium with its underground is not properly known. *Wieringa (1993)* presented in his study an equation to calculate the fetch that is required for the lowest 10 % of the internal boundary layer flow to be in equilibrium

$$x_{fetch} = 2z_{02}\left[\frac{10(z-z_{d2})}{z_{02}}\left(\ln\left(\frac{10(z-z_{d2})}{z_{02}}-1\right)\right)+1\right] \qquad (4.1)$$

with z_{02} the effective roughness length and z_{d2} the displacement thickness of the new roughness

behind the step. Applied to urban areas, this formula results in fetches of many km which does not seem to be realistic. MIHU started a focussed experimental programme under controlled conditions in a boundary layer wind tunnel in order to clarify the situation.

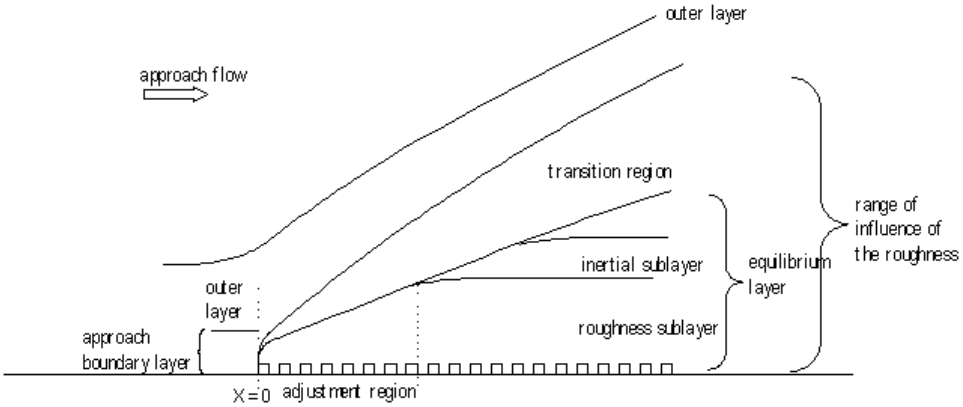

Fig. 4.2.1. Conceptual sketch of the flow development after a step change of roughness (modified from *Cheng & Castro, 2002*).

4.3. Experimental set-up

The experiments are carried out in MIHU's boundary layer wind tunnel "Blasius". The wind tunnel has a total length of 16 m and a test section which is 1.5 m wide and 1 m high. The tunnel is equipped with an adjustable ceiling (Fig 4.3.1).

An array of regularly arranged, sharp-edged wooden cubes was mounted on the tunnel floor. The development of the boundary layer above the cubes was investigated by measuring vertical profiles of the longitudinal and vertical velocity components u and w. The measurements were carried out using a DANTEC-LDA fibre probe. The probe had a focal length of 50 mm, the measurement volume had the dimension dx = 0.121 mm, dy = 0.122 mm, and dz = 1.151 mm.

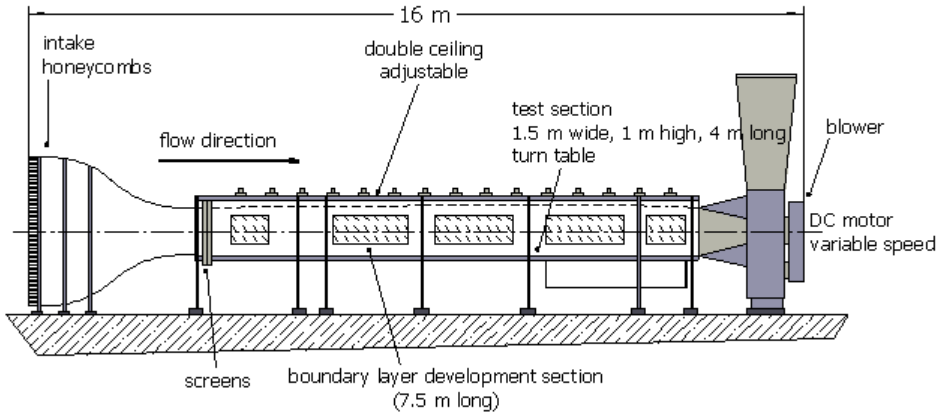

Fig. 4.3.1 Schematic sketch of the boundary layer wind tunnel "Blasius" at the Meteorological Institute of Hamburg University.

4.4. Experiments

The first series of measurements aimed at getting some general indications. Uniform, sharp-edged cubes with a height of h = 25 mm were grouped into 38 rows and mounted on the tunnel

floor (Fig. 4.4.1). The spacing between the cubes (= aspect ratio) varied from 0.5h over 1h to 2h. The tunnel floor upstream of the cubes was smooth. The vertical distribution of the flow approaching the cube array followed a power law profile:

$$\frac{\overline{u}(z)}{u_{ref}} = \left(\frac{z - z_d}{z_d} \right)^{\alpha} , \tag{4.2}$$

with profile exponent α = 0.16 and displacement thickness z_d = 0 mm. Spires or other devices to trigger the approach flow were not used. The flow development was solely regulated by the roughness elements. For the cube array, the Reynolds number criterion for fully rough flows was well fulfilled.

Along the centre-line of the cube array vertical profiles of mean velocities and turbulent intensities were measured with a horizontal resolution of 50 mm in order to study the development of the flow behind the roughness step.

Due to the rapid change in roughness height, there was a lift-up of the boundary layer flow to the elevation of the cube height. A long transition region was observed. Equilibrium seems to occur only at the lowest height investigated (z = 2.8h). At higher elevations neither the mean nor the turbulent properties reached equilibrium over the distance covered by the 38 rows of cubes. Fig. 4.4.2 shows the example of the development of the longitudinal turbulent intensities with distance from the roughness step and height above ground for 3 different aspect ratios. The influence of the particular aspect ratios seems to be small over the range investigated.

In order to acquire knowledge about the vertical profiles of mean and turbulent properties and on the variation of those profiles as a function of horizontal distance from an individual cube, a group of 9 cubes at the end of the cube array (behind row 32) was selected (black marked cubes in Fig. 4.4.2). For each of the 3 aspect ratios under consideration here, velocity time series were measured at about 20 positions relative to an individual cube and at about 25 vertical positions. The positions at which the profiles were measured are shown in Fig. 4.4.3.

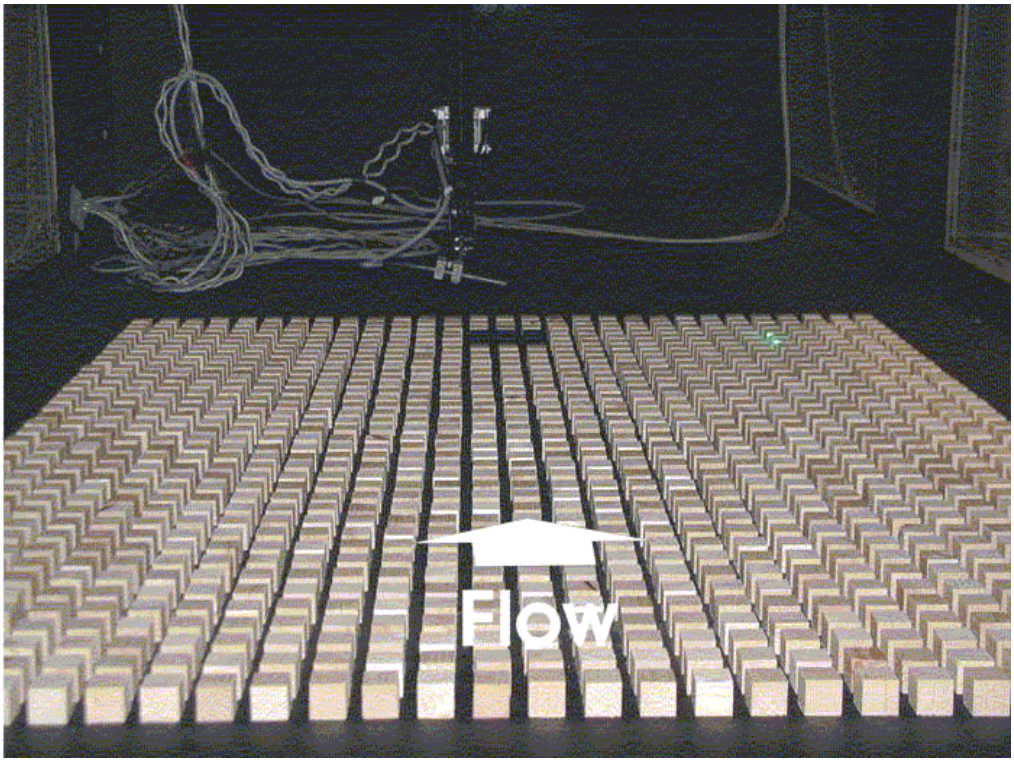

Fig. 4.4.1. Array of cubes in the wind tunnel.

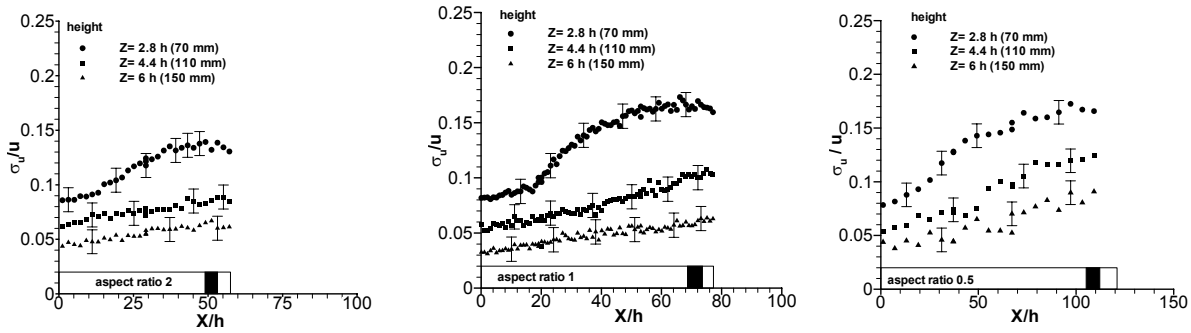

Fig. 4.4.2. Development of the longitudinal turbulent intensity σ_u/u with distance and height for cubes with identical height but different spacing (aspect ratios of 2 (left), 1 (middle), and 0.5 (right)).

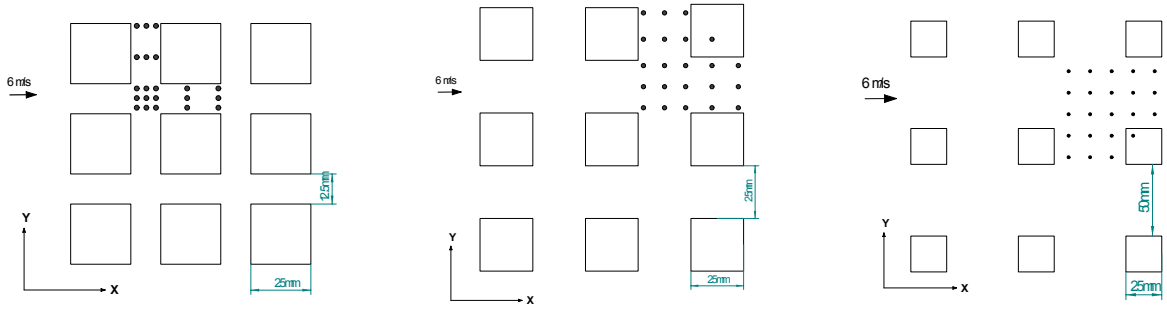

Fig. 4.4.3. Schematic sketch of the position of the measured profiles above the black marked array for aspect ratios of 2 (left), 1 (middle), and 0.5 (right).

The velocity time series were processed and the mean velocity components u and w, the turbulent intensities σ_u and σ_w and the vertical momentum flux $-\overline{u'w'}$ were computed. The results are shown in Figs. 4.4.4-4.4.6 for the three aspect ratios investigated. All velocities were normalized with the reference wind speed u_{ref}, measured well above the boundary layer in the free stream at z = 15.6h.

Included into the figures is the height and position of the roughness sublayer (RS) and of the inertial sublayer (IS). They were derived from the average over all individual vertical momentum flux profiles. According to *Cheng & Castro (2002),* the upper edge of the roughness sublayer is reached at the position where the momentum flux profiles taken at different positions relative to the roughness elements converge. The inertial sublayer is defined as the region within which the momentum fluxes vary less than 5 %. Other possible ways to determine the inertial sublayer as, e.g., fitting the logarithmic law to the mean velocity profiles are less stringent but give similar results.

All three figures show that the height of the roughness layer is about the same (= 1.5h), independently of the aspect ratio. In contrast to that, the height of the inertial sublayer seems to depend on the roughness spacing. Above all for the low density roughness array (aspect ratio = 0.5) the vertical extent of the inertial sublayer was found to be significantly smaller.

In corresponding field measurements, *Rotach (1993)* and *Oikawa & Meng (1995)* defined the upper limit of the roughness sublayer as the height at which the vertical momentum flux profile

reaches its maximum. Our measurements show that this criterion is not very practical. Depending on the position relative to the cube at which the profile is taken, the momentum flux can increase, be constant or decrease inside the roughness layer.

Another way to determine the influence of the aspect ratio on the flow characteristics above the roughness elements is to compare spatially averaged profiles. Fig. 4.4.7 shows the results.

The profiles of the mean wind speed u for the cube arrays with aspect ratio 2 and 1 have the same shape, but the profile measured over the cube array with aspect ratio 1 is slightly shifted to lower wind speeds. The gradient of these two profiles is the same. The profile of the cube array with aspect ratio 0.5 has a different gradient in wind speed up to the level $z = 7h$. Above this level all three profiles lie within the scatter band. This indicates that free stream conditions have been reached at this level. The shape of the three w-profiles for the three different cases is similar with a tendency towards higher values for less densely packed cube arrays. However, the measured values are near to detection limit of the LDA system and lie more or less inside the scatter band. The turbulent flux profiles (Fig. 4.4.7e) for the arrays with aspect ratio 1 and 0.5 fall nearly on top of each other whereas those for the roughness with aspect ratio 2 are smaller, above all near to the roughness elements. The shape for this profile seems to be similar to that found by *Rotach (1993)* who, however, reported an aspect ratio of about 1 for the street canyon where his measurements were accomplished. It appears, that approach flow conditions are found above $z = 6h$ for the profiles above the arrays with aspect ratio 0.5 and 1 and for the last cube array above the height $z = 9$h. The same applies for profiles of the standard deviations σ_u and $\sigma_{w.}$

The cube arrays with aspect ratio 2 and 1 had a very similar influence on the mean velocity components. These rather densely packed roughnesses behaved more like sand roughness whereas the cube array with aspect ratio 0.5 showed features of individual obstacles. With respect to turbulence there were more similarities between the cube arrays with aspect ratio 1 and 0.5. Both arrays generate more turbulence through the individual obstacle than it was found in the experiments with the dense packed array. Also, the turbulence generated by the cube array with aspect ratio 0.5 reaches to higher elevations than the two others.

4.5. Findings of the experiments

The series of measurements in this report was done with a roughness change from smooth to very rough. This rapid change in ground roughness is probably not the best approximation to reality. The flow approaching the cube array is of comparatively low turbulence intensity. The disturbance of the boundary layer caused by the roughness step is so severe that even a fetch of 33 rows of roughness elements occurs to be not enough to regain equilibrium over the boundary layer.

Therefore, a second series of measurements has been started. Two changes compared to the present experiments will be made:

- First, the fetch upstream from the intensive measurement area will be about doubled to ensure the boundary layer to be in equilibrium with the surface conditions.
- Secondly, the approach flow will be made significantly more turbulent by using an appropriate set of vortex generators. This scenario is closer to real atmospheric conditions. It is expected that vertical mixing is enhanced, with the consequence that equilibrium is attained after a shorter fetch.

a)

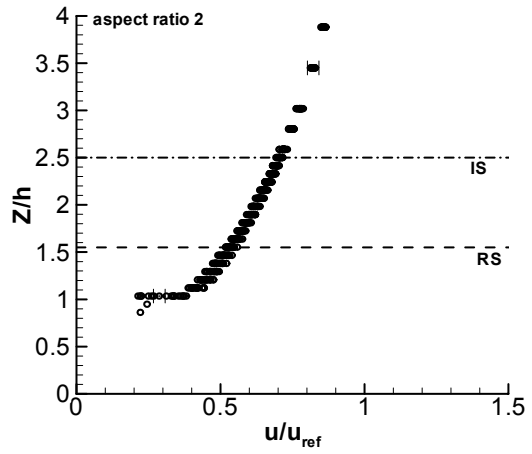

b)

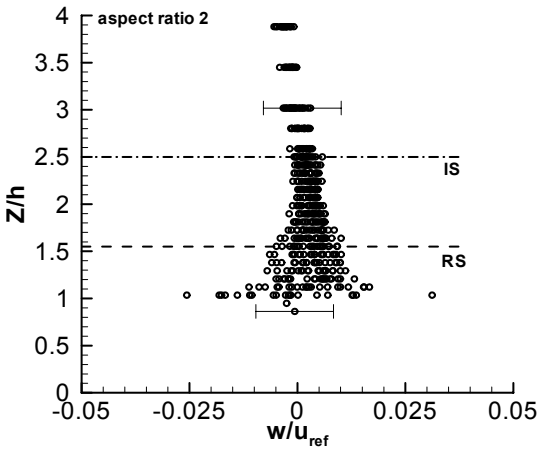

c)

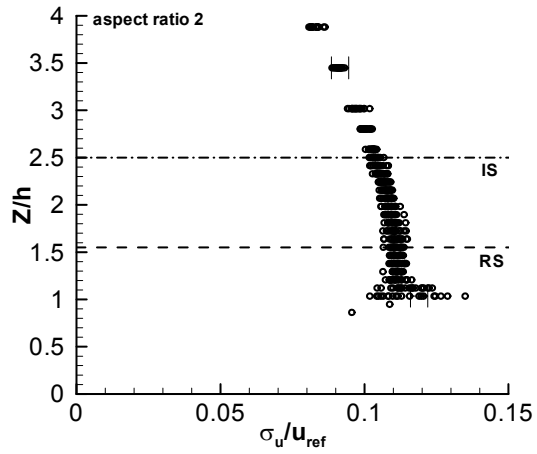

d)

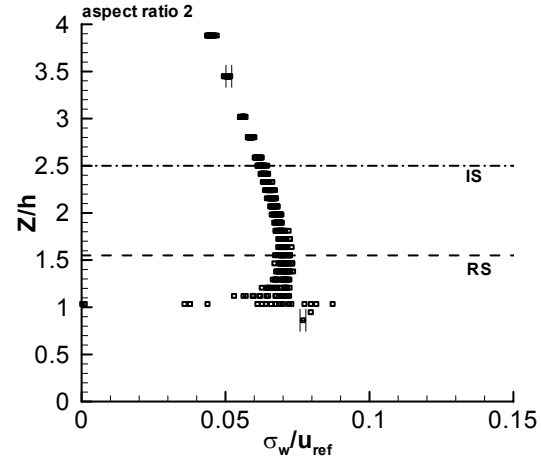

e)

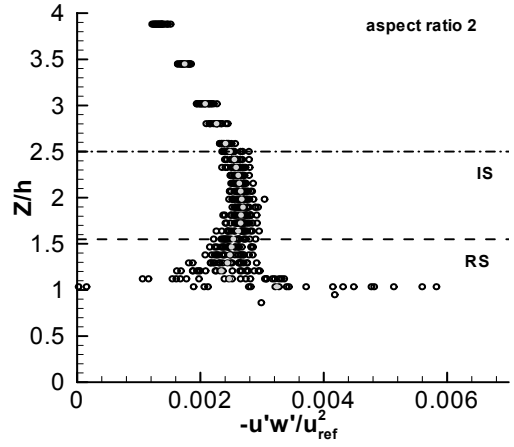

Fig. 4.4.4. Profiles above the black marked field for the cube array with aspect ratio 2 (error bars indicate reproducibility).

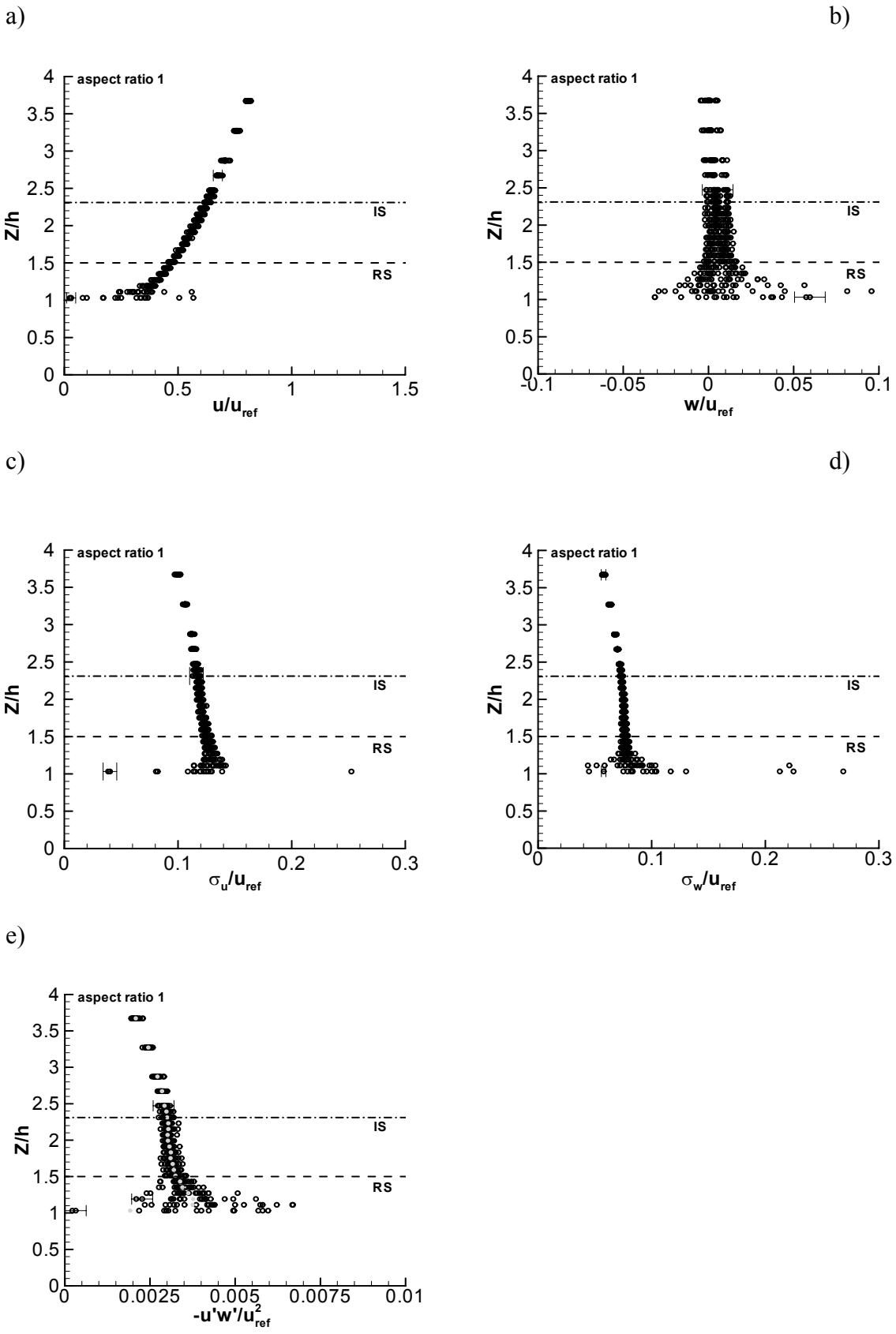

Fig. 4.4.5. Profiles above the black marked field for the cube array with aspect ratio 1 (error bars indicate reproducibility).

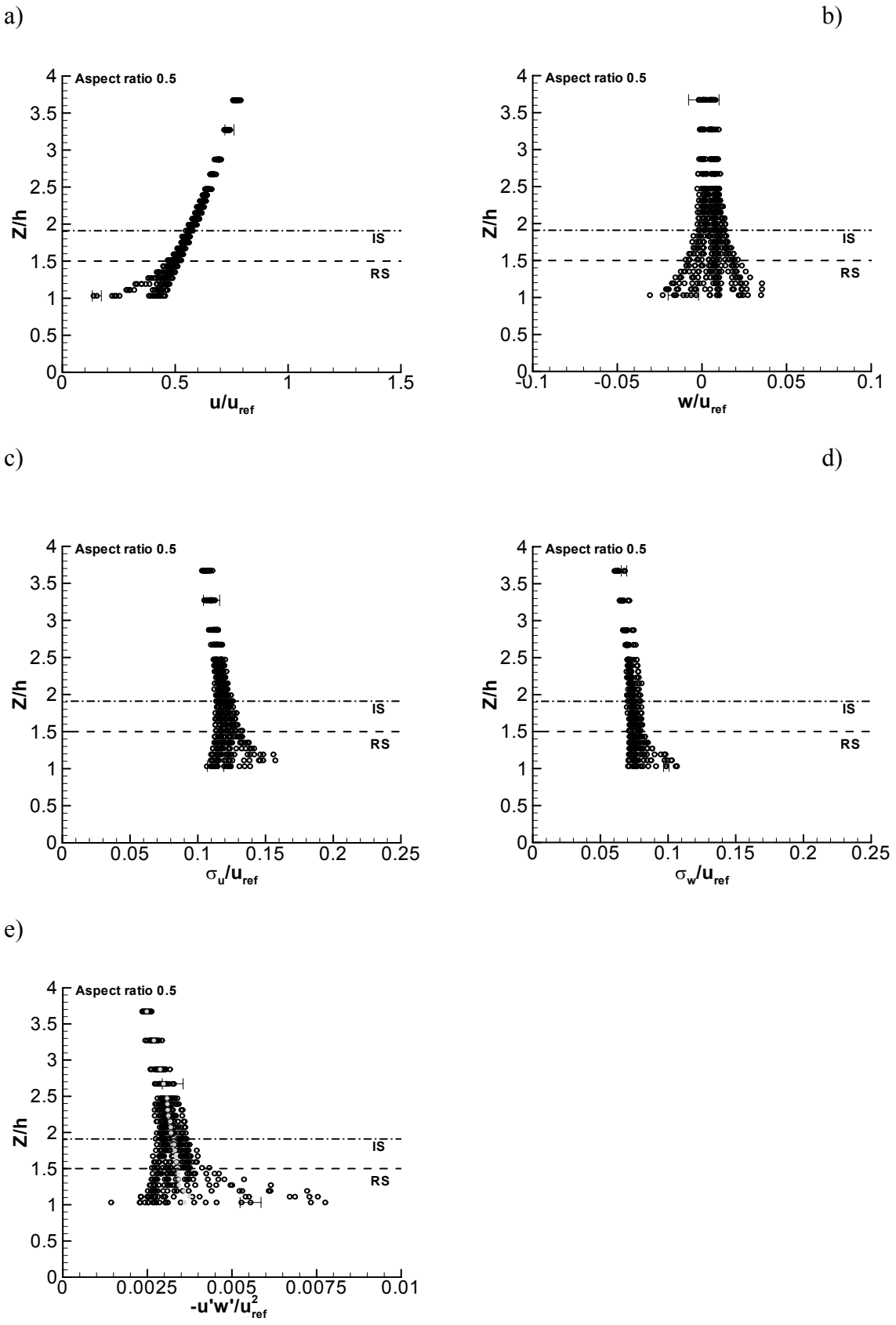

Fig. 4.4.6. Profiles above the black marked field for the cube array with aspect ratio 0.5 (error bars indicate reproducibility).

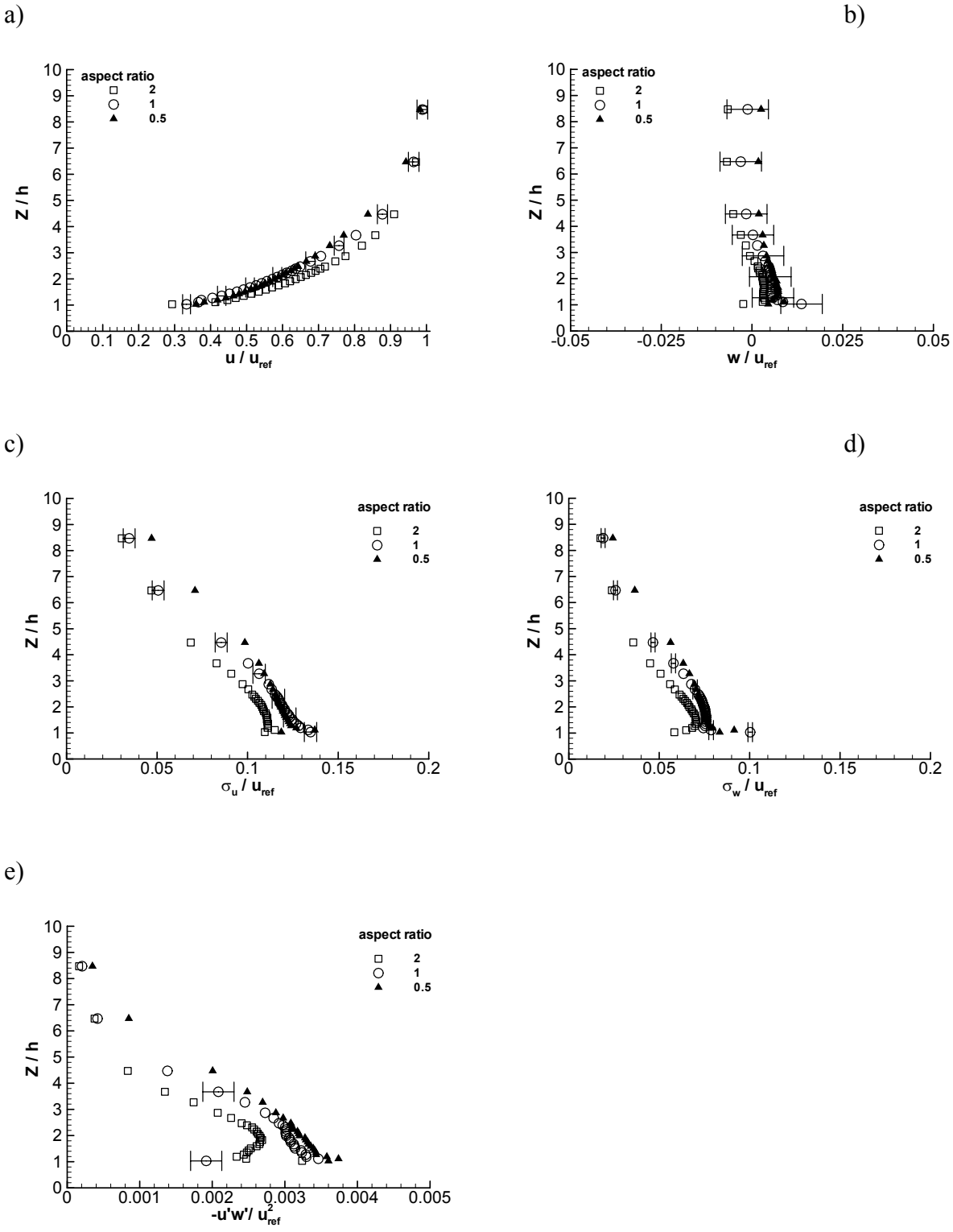

Fig. 4.4.7. Comparison of spatially averaged profiles with aspect ratios 2, 1 and 0.5 error bars indicate the measurement accuracy).

4.6. Ongoing and planned experiments for Basle roughness canopy

FUMAPEX intends to apply high-resolution NWPs to urban sites. However, in these models the parameterisations used for the lowest layers (roughness sublayer and inertial sublayer) are presently not adequate. In order to improve the situation, the Swiss partner (ETH, partner 16) carried out field measurements in the city of Basle, Switzerland. Profiles of mean and turbulent meteorological properties were measured within and above the building structure. In addition, tracer gas experiments were carried out.

Field data usually exhibit large scatter. They consist of a collection of data taken under random weather conditions. Systematic dependencies between particular variables that form the basis for good parameterisations are not easily detectable. Therefore, selected episodes from the field experiments will be repeated under carefully controlled conditions in MIHU's large boundary layer wind tunnel 'WOTAN' (Fig. 4.6.1). This work has started, first measurements have been made but the data are not yet completely processed.

The Basle "roughness" is comparatively uniform, but that is rather untypical for European conurbations. More common are complex and distinctly non-uniform canopy layers as shown in Fig. 4.6.2 for the example of Frankfurt/Germany. The height of buildings (= roughness elements) continuously varies, and the boundary layer needs to adjust to ever-changing conditions. Since the flow field is not in equilibrium with the surface roughness, the universal relationships for the vertical distribution of mean and turbulent properties (which form the core of roughness parameterisations!) cannot simply be derived from local profile measurements.

The experiments are ongoing. The results will be presented in the next progress report.

Figure 4.6.1. Model of Basle in MIHU's boundary layer wind tunnel 'WOTAN'. Selected episodes from a field campaign carried out by partner 16 (ETH) will be repeated under controlled ambient conditions.

Figure 4.6.2. Example of a typical non-uniform urban canopy layer (Frankfurt/Germany).

5. Conclusions

1. The urbanisation strategy of FUMAPEX includes the following three levels of complexity: a) urban roughness/fluxes and increased resolution; b) effective roughness and flux aggregation techniques; c) urban sublayer and soil model.

2. According to the deliverable D4.4: 'Improved models for computing the roughness parameters of urban areas' the first step of the strategy for the urbanisation of NWP models in FUMAPEX, including the improvement of spatial resolution, nesting of NWP models and urban roughness calculation, is realised.

3. Increased resolution and surface data-bases for the roughness length calculation in operational NWP models are considered and tested in DMI-HIRLAM, LM, MM5 and RAMS models, used by the FUMAPEX partners.

4. Modified parameterizations and algorithms for roughness parameters in urban areas based on the morphologic methods are developed. Urban database analysis for mapping morphology and aerodynamic parameters is tested against the St. Jerome case study, ESCOMPTE.

5. Improved models for urban roughness sublayer simulation, including (i) Effective roughness and flux aggregation technique, (ii) Effect of stratification on the surface resistance over very rough surfaces, (iii) Roughness for momentum, heat, and moisture, are suggested.

6. It was shown that the roughness length depends on the atmospheric temperature stratification, new parameterisations for the effect of stratification on the surface resistance over very rough surfaces are suggested. The roughnesses for momentum, temperature and moisture are different for urban areas. Several possible parameterisations for the scalar roughness length for urban areas are recommended for urban-scale NWP models, they need to be verified and improved.

7. As the next step for the NWP urbanisation it is suggested to parameterise the urban roughness sub-layer by the Martilli model. This method is more advanced than the roughness approach, but more expensive for computing in NWP.

8. Experimental study of urban roughness inhomogeneity effects on the UBL development is realised and the results are made available for model verifications.

References

Arya S.P.S., 1975. Buoyancy effects in a horizontal flat-plate boundary layer, *J. Fluid Mechanics*, 68, 321-343

Astrup, P., Jensen, N.O., Mikkelsen, T., 1996: Surface roughness model for LINCOM. Risø-R-900(EN), 30 p.

Baklanov, A. (ed.), 2003: FUMAPEX Integrated Systems for Forecasting Urban Meteorology, Air Pollution and Population Exposure – Project Kick-off Meeting and First Progress Report, *DMI Scientific Report 12/03, ISSN 0905-3263*. URL: http://www.dmi.dk/f+u/publikation/vidrap/2003/Sr03-12.pdf

Baklanov, A., A. Rasmussen, B. Fay, E. Berge and S. Finardi, 2002: Potential and Shortcomings of Numerical Weather Prediction Models in Providing Meteorological Data for Urban Air Pollution Forecasting. *Water, Air and Soil Poll.: Focus*, **2**(5-6): 43-60.

Baklanov, A., J.H. Sørensen, S. Hoe, B. Amstrup. 2003: Urban Meteorological Modelling for Nuclear Emergency Preparedness. NKS Conference on Radioactive Contamination in Urban Areas, May 7-9, 2003, Risø, Roskilde, Denmark. *J. Envir. Radioactivity* (submitted)

Belcher, S.E., O. Coceal, 2002: Scaling the urban boundary layer. COST 715 Zurich Workshop.

Belcher, S.E., Jerram, N., Hunt, J.C.R., 2003: Adjustment of the turbulent boundary layer to a canopy of roughness elements. Under consid. For publication in J.Fluid Mech., 30pp.

Berge, E., Walker, S-E., Sorteberg, A., Lenkopane, M., Eastwood, S., Jablonska, H.I. and Køltzow, M.Ø., 2002. A real-time operational forecast model for meteorology and air quality during peak air pollution episodes in Oslo, Norway. *Water, Air and Soil Pollution Focus* 2, Urban Air Quality - Recent Advances, pp 745-757.

Bornstein, R. D. (2001). Currently used parameterisations in numerical models. Workshop on Urban Boundary Layer Parameterisations. COST 715, Zürich, May 24-25 2001.

Bottema, M. and P.G. Mestayer: 1998, Urban roughness mapping - validation techniques and some first results, *J. Wind Engineering & Industrial Aerodynamics*, **74-76**, 163-173

Bottema, M., 1997: Urban roughness modelling in relation to pollutant dispersion,. *Atmos. Env.*, **31**, 3059-3075.

Bottema, M., W. Klaassen and W.P. Hopwood: 1998, Landscape roughness parameters for Sherwood Forest - validation of aggregation models, *Boundary-Layer Metorol.*, **89**, 317-347

Bottema, M.: 1995, Aerodynamic roughness parameters for homogeneous building groups - Part 1: Theory, Document SUB-MESO # 18; Part 2: Results, Document SUB-MESO # 23, (Ecole Centrale de Nantes, France)

Bottema, M.: 1996, Roughness parameters over regular rough surfaces: Experimental requirements and model validation, *J. Wind Engineering & Industrial Aerodynamics*, **64**, 249-265

Brutsaert W., 1975: The Roughness Length for Water Vapor, Sensible Heat, and Other Scalars. *Journal of Atmospheric Sciences*, Vol 32, pp. 2028-2031.

Businger, J. A.: 1975, Aerodynamics of vegetated surfaces. Heat and Mass transfer in the Biosphere I heat transfer in the plant environment, D.A. de Vries, N.A. Afgan, eds., 139-165

Calanca P., 2001: A Note on the Roughness Length for Temperature over Melting Snow and Ice. *Q.J.R. Meteorological Society*, Vol 127, pp. 255-260.

Cheng , H. , Castro, I.,P. 2002: Near-Wall Flow Development after a Step Change in Surface Roughness, *Boundary- Layer Meteorology* **105**, 411-432

Cheng , H. , Castro, I.,P. 2002: Near-Wall Flow over Urban-Like Roughness, *Boundary-Layer Meteorology* **104**, 229-259

Clean City Air (1999) Status report: Development and testing of a pilot model for air quality in Oslo and Bergen. Results from Oslo. DNMI, Norway.

COST-715: 2001, 'Surface energy balance in urban areas', Extended abstracts of an Expert Meeting. WG-2 COST Action 715, Antwerp, Belgium, 12 April 2000. European Commission, EUR 19447.

COST-715: 2002, Workshop on urban boundary layer parameterisations. Extended abstracts. WG-1&2 COST Action 715, Zurich, Switzerland, 24-25 May 2001. European Commission, EUR20355.

Counihan, J.: 1971, Wind tunnel determination of the roughness length as a function of the fetch and the roughness density of three-dimensional roughness elements, *Atmospheric Environment* , **5**, 637-642

Daniel, M., J. Hameon: 1996, Un logiciel de creation de cartes de rugosite, *Le courrier du CNRS,* **82**, 95-97 (English translation available, CNRS, France)

Davenport, A., S. Grimmond, T. Oke and J. Wieringa: 2000, The revised Davenport roughness classification for cities and sheltered country, *3rd Symp. On the Urban Environment*, 14-18 Aug. 2000, Davis, Ca, AMS Proceedings, 9-10

De Rider, K. 2003: Horisontal scale of roughness variations for realistic landscapes. *Boundary-Layer Meteorol*., **109**, 49-57.

De Rider, K. 2003: Remote sensing of the urban surface energy balance. Chapter 6 in WG2 COST715 Report (manuscript).

Doms, G., Schättler, U. (1999): The nonhydrostatic limited-area model LM, part1: scientific documentation. R&D Dep. of DWD, 169p.

Dupont, S., I. Calmet and P. Mestayer, 2002: Urban canopy modelling influence on urban boundary layer simulation, 4th AMS Symposium on Urban Climatology, 20-24 May 2002, Norfolk, VA, Proceedings AMS, pp. 151-152

Dupont, S., E. Guilloteau & P.G. Mestayer, 2000: Energy balance and surface temperatures of urban quarters, 3rd AMS Symposium on Urban Environment, Davis, California, 14-18 August 2000 , AMS proceedings pp. 149-150.

Dupont, S., I. Calmet, P.G. Mestayer and S. Leroyer, 2003: Parameterisation of the Urban Energy Budget with the SM2-U Model for the Urban Boundary-Layer Simulation, submitted to *Boundary Layer Meteorology*, September 2003

Dupont, S. E. Guilloteau, P.G. Mestayer, E. Berthier and H. Andrieu, 2003: Parameterisation of the Urban Water Budget by Using SM2-U model, submitted to *Journal of the Applied Meteorology*, August 2003

Esau, I., 2003: University of Uppsala. Personal communications.

ESDU, 1985: Characteristics of Atmospheric Turbulence near the Ground, *Engineering Sciences Data Unit,* Item No. 85020, London

Fay, B., 2003: Overview of NPW / wind field models in FUMAPEX. Internal FUMAPEX Report (contr. EVK4-CT-2002-00097), WP3: Testing the quality of different operational meteorological forecasting systems for urban areas, Deliverable D3.1. Deutscher Wetterdienst, Offenbach.

Feigenwinter, C. **,** Vogt, R. **,** Parlow, E. 1998: Vertical Structure of Selected Turbulence Characteristics above an Urban Canopy, *Theoretical Applied Climatology*, **62**, 51-63

Fisher B.E.A., Erbrink J.J, Finardi S., Jeannet P., Joffre S., Morselli M.G., Pechinger U., Seibert P. and Thomson D.J.: 1998, Harmonisation of the Pre-processing of Meteorological Data for Atmospheric Dispersion Models. COST Action 710 – Fin. Rep., EUR 18195.

FUMAPEX: EU 5FP project "Integrated Systems for Forecasting Urban Meteorology, Air Pollution and Population Exposure", contract # *EVK4-2001-00281* (Nov 2002 – Oct 2005). Project web-page: http://fumapex.dmi.dk

Garratt, J.R. 1990: The internal Boundary Layer – A Review, *Boundary- Layer Meteorology* **50**, 171-203

Garratt J.R., 1992: The Atmospheric Boundary Layer. *Cambridge University Press*, UK.

Garratt J.R. and B.B. Hicks, 1973. Momentum, heat and water vapour transfer to and from natural and artificial surfaces. Q.J.R.Met. Soc. 99, 680-687.

Grachev, A. A., Fairall, C. W., and Zilitinkevich, S. S. (1997) Surface-layer scaling for the convection-induced stress regime. *Boundary-Layer Meteorol*., **83**, 423 - 439.

Grell G A, Dudhia J and Stauffer D R A 1995: Description of the Fifth-Generation Penn State/NCAR Mesoscale Model (MM5), NCAR Tech. Note, NCAR/TN-398 + STR, 122 pp.

Grimmond CSB., Oke T., 1999: Aerodynamic properties of urban area derived from analysis of surface

form, in *Journal Applied Meteorology*, 38, pp.1261-1292.

Grimmond, C.S.B., T.S. King, M. Roth and T. Oke: 1998, Aerodynamic roughness of urban areas derived from wind obsevations, *Boundary-Layer Metorol.*, **89**, 1-24

Gryning, S.-E. and E. Batchvarova (2001). *Mixing height in urban areas: will "rural" parameterisations work?* COST-Action 715 Workshop on Urban Boundary Layer Parameterisations. Zürich, May 24-25 2001, 10 p.

Guilloteau E. and Mestayer, P.G.: 2000, Numerical simulations of the urban roughness sublayer: a first attempt, J. Env. Monit. a. Assess. 65, 1/2, pp. 211--219.

Guilloteau, E.: 1999, Modelisation des sols urbains pour les simulations de l'atmosphere aux echelles sub-meso. Doctorate thesis, Universite & Ecole Centrale de Nantes, France

Gustavsson, N., Berre, L., Hörnquist, S., Huang, X.-Y., Lindskog, M., Navascues, B., Mogensen, K.S., Thorsteinsson, S., 2001, Three-dimentional variational data-assimilation for a limited area model. Part I: General formulation and the background error constraint. *Tellus*, **53A**: 425-446.

Gutman, G., and A. Ignatov, 1998: The derivation of the green vegetation fraction from NOAA/AVHRR data for use in numerical weather prediction models. *Int. J. Remote Sensing*, **19**, 1533 – 1543.

Hanna, S.T. and J.C. Chang: 1992, Boundary layer parameterizations for applied dispersion modelling over urban areas, *Boundary-Layer Metorol.*, **58**, 229-259

Hasager C.B., Jensen N.O., 1999: Surface-Flux Aggregation in Heterogeneous Terrain. *Q.J.R. Meteorological Society*, Vol 125, pp. 2075-2102.

Hasager, C.B. Nielsen, N.W., Boegh, E., Jensen, N.O., Christensen, J.H, Dellwik, E. and Soegaard, H., 2003: Effective roughnesses calculated from satellite-derived land cover maps and hedge information and used in a weather forecasting model. *Boundary-Layer Meteorology,* 109: 227-254.

Hasager, C.B. Nielsen, N.W., H. Soegaard, Boegh, E., Christensen, J.H, Jensen N.O., M.S. Rasmussen, P. Astrup, E. Dellwik, 2002: SAT-MAP-CLIMATE Project Results. *Riso National Laboratory Report, Riso-R-1350(EN),* Roskilde, Denmark, Aug 2002, ISBN-87-550-3079-3, 71p.

Hasager, C.B.; Thykier-Nielsen, S., 2001: IRS-1C LISS III land cover maps at different spatial resolutions used in real-time accidental air pollution deposition modelling. *Remote Sens. Environ.*, **76** , 326-336

Herzog, H.-J., Schubert, U., Vogel, G., Fiedler, A., Kirchner, R. (2002): LLM – the high-resolving nonhydrostatic simulation model in the DWD - Project LITFASS Part I: Modelling technique and simulation method. COSMO Tech. Rep. No. 4, 68pp., download from www.cosmo-model.org.

Herzog, H.-J., Vogel, G., Schubert, U.(2002b): LLM – a nonhydrostatic model applied to high-resolving simulations of turbulent fluxes over heterogeneous terrain. Theor. Appl.Climat. 73,67-86.

Högström, U., 1995: Review of some basic characteristics of the atmospheric surface layer. *Boundary-Layer Metorol.*, **78**, 215-246

Högström, U. , Bergström, H. , Alexandersson, H. 1982: Turbulent characteristics in a near neutrally stratified urban atmosphere, *Boundary- Layer Meteorology*, **23**, 449-472

Hoppwood, W.P., 1996: Observations and Parameterisation of Momentum Transfer in Heterogeneous Terrain Consisting of Regularly Spaced Obstacles, *Boundary- Layer Meteorology*, **81**, 217-243

Hunt, J. C. R., Kaimal, J. C., and Gaynor, J. I. (1988) Eddy structure in the convective boundary layer - new measurements and new concepts, *Quart. J. Roy. Meteorol. Soc*. **114**, 837-858.

Hussain, M.: 1978, A study of the wind forces on low rise building arrays and their application to natural ventilation design methods, PhD thesis, University of Sheffield, UK

Jensen, N.O., Hasager, C.B. and Larsen, S.E., 2002: Aggregation of momentum and temperature roughness based on satellite data. EGS XXVII General Assembly, Nice, France, 21-26 April, *Geophys. Research. Abstracts.*

Joffre S.M., 1982: Momentum and Heat Transfers in the Surface Layer over a Frozen Sea. *Boundary Layer Meteorology*, Vol 24, pp. 211-229.

Joffre S.M., 1988. Modelling the Dry Deposition Velocity of Highly Soluble Gases to the Sea Surface. *Atmos. Environ*., **22**(6), p. 1137-1146

Kader, B. A., and Yaglom, A. M. (1990) Mean fields and fluctuation moments in unstably stratified turbulent boundary layers, *J. Fluid Mech*. **212**, 637-662.

Källen, E., 1996, HIRLAM documentation manual, System 2.5. Available from SMHI, Norrköping, Sweden.

Kastner-Klein, P. 2000: Overview of Near-Surface Turbulence Parameterisations, *Proceedings of the COST 715 Workshop,* Prag, 31-40

Kastner-Klein, P., E. Fedorovich and M. W. Rotach, 2001: A wind tunnel study of organized and turbulent air motions in urban street canyons. *J. Wind Engineering Industrial Aerodynamics*, **89**, 849-861.

Kondo, J. and H. Yamazawa: 1986, Aerodynamic roughness over an inhomogeneous ground surface, *Boundary-Layer Metorol.*, **35**, 331-348

Kukkonen, J. (ed.), 2001. COST action 715, Meteorology applied to Urban Air Pollution Problems, Working Group 3, Status Report. Directorate-General for Research, Information and Communication Unit, European Commission. Brussels, 73 pages.

Kusaka, H., H. Kondo, Y. Kikegawa and F. Kimura, 2001: Asimple single-layer urban canopy model for atmospheric models: Comparison with multi-layer and SLAB models, *Boundary Layer Meteorol.,* **101**, 329-358.

Kutzbach, J.: 1961, Investigations of the modifications of wind profiles by artificially controlled surface roughness. Studies of the three-dimensional structure of the planetary boundary layer. Annual report. Dep. Meteorology. Univ. Wisconsin, Madison

Lettau, H.: 1969, Note on aerodynamic roughness-parameter estimation on the basis of roughness-element description,. *J. Applied Met.*, **8**, 828 - 832

Long N. 2003: Analyses morphologiques et aérodynamiques du tissu urbain – Application à la climatologie urbaine de Marseille pendant la campagne ESCOMPTE. *Doctoral Thesis* (in French), Université des Sciences et Techniques de Lille, Dec 2003, 297 p.

Long N., S. Kermadi, C. Kergomard, P. Mestayer, A. Trobouet, 2003a: Urban cover modes and thermodynamic parameters from urban database and satellite data: a comparison for Marseille during ESCOMPTE. *Proceedings of the 5th International Conference on Urban Climate*, 1-5 Sep 2003, Lodz, Poland, CD # 0.5.2.

Long N., P. Mestayer, C. Kergomard, 2003b: Urban database analysis for mapping morphology and aerodynamic parameters: the case of St. Jerome sub-urban area, in Marseille during ESCOMPTE. *Proceedings of the 5th International Conference on Urban Climate*, 1-5 Sep 2003, Lodz, Poland, CD # 0.31.3.

Long N., P.G. Mestayer, C. Kergomard, 2002: Development of a software to describe the city morphology and to compute aerodynamic parameters from an urban data base. *Proceedings of the 4th symposium on Urban Climatology*, American Meteorological Society, 20-24 May 2002, Norfolk, pp.31-32.

Macdonald R.W., Griffiths R.F., Hall D.J., 1998: An improved method for estimation of surface roughness of obstacle arrays. *Atmospheric Environment*, 32, pp. 1857-1864.

Macdonald, R.W. 2000: Modelling the Mean Velocity Profile in the Urban Canopy Layer, *Boundary-Layer Meteorology,* **97**, 25-45

Macdonald, R.W., Carter scholfield, S., Slawson, P.R. 2002: Physical Modelling of Urban Roughness Using Arrays of Regular Roughness Elements, *Water, Air and Soil Pollution: Focus* **2**, 541-554

Mahrt L. and Ek M., 1993: Spatial Variability of Turbulent Fluxes and Roughness Lengths in HAPEX-MOBILHY. *Boundary Layer Meteorology*, Vol 65, pp. 381-400.

Martilli, A., A. Clappier, and, M. W. Rotach, 2002: An urban surfaces exchange parameterisation for mesoscale models, *Boundary Layer Meteorol.,* **104**, 261-304.

Mason P., 1988: The Formation of Areally-Averaged Roughness Lengths. *Q.J.R. Meteorological Society*, Vol 114, pp. 399-420.

Masson, V., 2000: A physically-based scheme for teh urban energy budget in atmospheric models, *Boundary Layer Meteorol.,* **94**, 357-397.

Mellor, G.L., Yamada, T.(1974): A hierarchy of turbulence closure models for planetary boundary layers.

J.Atm. Sc., 31,1791-1806.

Mestayer, P.G., M. Bottema, J.-P. Costes and J.-F. Sini: 1997, Modelling urban canopy and terrain for transport-diffusion simulations at sub-mesoscales, *Int. J. Environment and Pollution*, **8**, 675-682

Mestayer, P.G.: 1998, Urban Scale Models, *Urban air pollution - European aspects*, Kluwer Acad. Public., Dordrecht, Boston, London, 197-222

Mestayer, P.G., J.-P. Costes and J.-F. Sini, 2002: Inhomogeneous roughness influence on neutral atmospheric boundary layer simulation. Part I, steps, strips, and spots. Submitted to *Boundary-Layer Meteorology*, November 2002.

Mestayer, P.G., S. Dupont and J.-F. Sini, 2002: Inhomogeneous Roughness Influence on Neutral Atmospheric Boundary Layer Simulation. Part II, Regular Checkerboard'. Submitted to *Boundary-Layer Meteorology*, November 2002

Molder M., Lindroth A., 1999: Thermal Roughness Length of a Boreal Forest. *Agricultural and Forest Meteorology*, Vol 98-99, pp. 659-670.

Molder M., Sigute M., Hiyama T., Bergstrom H., 1998: Regional Sensible Heat Flux and Thermal Roughness Length of an Inhomogeneous Landscape. *Hydrological Processes*, Vol 12, pp. 2115-2131.

Monin, A. S., and Yaglom, A. M. (1971) *Statistical Fluid Mechanics*. Vol. 1, MIT Press, Cambridge MA, 769 pp.

Müller, W.,J., Heits, B., and Schatzmann, M. (2002): A Prototype Station for the Collection of Urban Meteorological Data. Proceedings, 8th International Conference on Harmonisation within Atmospheric Dispersion Modelling for Regulatory Purposes, Sofia, Bulgaria, October 14-17.

NLÖ, 1995: Lufthygienisches Überwachungssystem Niedersachsen – Standortbeschreibung der NLÖ Stationen. Bericht, Niedersächsisches Landesamt für Ökologie, Göttinger Str. 14, 30449 Hannover (in German).

Oikawa, S. and Meng, Y., 1995: Turbulence Characteristics And Organized Motion in a Suburban Roughness layer, *Boundary- Layer Meteorology*, **74**, 289-312

Oke, T.R.: 1997, 'Urban environments', in *The Surface Climates of Canada,* Bailey, W.G., T.R. Oke and W.R. Rouse, Eds., McGill-Queen's University Press, Montréal, 303-327.

Oke, T.R., Spronken-Smith, R., Jauregui, E. and Grimmond, C.S.B.: 1999, 'Recent energy balance observations in Mexico City', *Atmos. Env.* **33**, 3919--3930.

Panofsky, H.A. , Dutton, J.A. 1984: Atmospheric Turbulence. *Wiley & Sons,* 397 S.

Parlow, E.: 1999, Remotely sensed heat fluxes of urban areas. Int. conf. on Biomet. and Urban Climatol. at the Turn of the Millennium, Sydney Australia, 8 – 12 Nov 1999, ICUC13.3.

Pielke R.A., Cotton W.R., Walko R.L., Tremback C.J., Lyons W.A., Grasso L.D., Nicholls M.E., Moran M.D., Wesley D.A., Lee T.J. and Copeland J.H. (1992) A Comprehensive Meteorological Modeling System - RAMS, Meteorol. Atmos. Phys. 49, 69-91.

Piringer, M, C S B Grimmond, S M Joffre, P Mestayer, D R Middleton, M W Rotach, A Baklanov, K De Ridder, J Ferreira, E Guilloteau, A Karppinen, A Martilli, V Masson, M Tombrou, 2002: Investigating the Surface Energy Balance in Urban Areas – Recent Advances and Future Needs. *Water, Air and Soil Poll.: Focus,* 2(5-6): 1-16.

Rafailidis, S.: 1997, Influence of building, areal density and roof shape on the wind characteristics above a town, *Boundary-Layer Metorol.*, **85**, 255-271

Raschendorfer, M. (1999): The new turbulence parameterization of LM. Quarterly Report of the Operational NWP-Models of the DWD, No 19, 3-12

Ratti, C.F., S. Di Sabatino, F. Caton and R.E. Britter: 2000, Morphological parameters for urban dispersion models, *3rd Symp. On the Urban Environment*, 14-18 Aug. 2000, Davis, Ca, AMS Proceedings, 9-10

Raupach, M.R. 1992: Drag and Drag Partition on Rough Surfaces, *Boundary- Layer Meteorology*, **60**, 375-395

Raupach, M.R. , Thom, A.S. , Edwards, I. 1979: A wind-tunnel study of turbulent flow close to regularly arrayed rough surfaces, *Boundary- Layer Meteorology*, **18**, 373-397

Raupach, M.R.: 1994, Simplified expressions for vegetation roughness length and zero-plane displacement height as functions of canopy height and area index, *Boundary-Layer Metorol.*, **71**, 211-216

Raupach, M.R.: 1995, Corrigenda, *Boundary-Layer Metorol.*, **76**, 303-304

Rotach, M. W., (2001): Urban scale dispersion using lagrangian stochastic dispersion model, *Boundary-Layer Meteor.*, **99**, 379-410.

Rotach, M.W. 1992: Turbulence Close to a Rough Urban Surface Part I: Reynolds Stress, *Boundary- Layer Meteorology*, **65**, 1-28

Rotach, M.W. 1993: Profiles of turbulence statistics in and above an urban street canyon, *Atmospheric Environment*, **29**, 1473-1486

Rotach, M.W. 1993: Turbulence Close to a Rough Urban Surface Part II: Variances and Gradients, *Boundary- Layer Meteorology*, **66**, 75-92

Rotach, M.W. 1999: On the influence of the urban roughness sublayer on turbulence and dispersion, *Atmospheric Environment*, **33**, 4001-4008

Rotach, M.W.: 1994, Determination of the zero-plane displacement in an urban area, *Boundary-Layer Metorol.*, **67**, 187-193

Roth, M. 1993: Turbulent Transfer Relationships over an Urban Surface Part I : Spectral Characteristics, *Quarterly Journal of the Royal Meteorological Society*, **119**, 1105-1120

Roth, M. 1993: Turbulent Transfer Relationships over an Urban Surface Part II : Integral Statistics, *Quarterly Journal of the Royal Meteorological Society*, **119**, 1071-1104

Roth, M. , Oke, T.R. Relative Efficiencies of Turbulent Transfer of Heat, Mass and Momentum over a Patchy Urban Surface, *Journal of the Atmospheric Sciences*, **52**, no. 11, 1863-1874

Roth, M. 1999: Review of Atmospheric Turbulence over Cities, *Quarterly Journal of the Royal Meteorological Society*, 126, no. 564, 941-990

Roth, M. and T. R. Oke (1993), Turbulent transfer Relationships over an Urban Surface I: Spectral characteristics, *Quart. J. Roy Meteorol. Soc.,* **119**, 1071-1104

Saito, K., Doms, G., Schaettler, U., Steppeler, J. (1998): 3-D mountain waves by the Lokal-Modell of DWD and the MRI mesoscale nonhydrostatic model. *Met. and Geophys*., Vol. 49, No.1, 7-19, Met. Res. Inst., Tsukuba, Ibaraki, Japan

Sass, B. H., N. W. Nielsen, J. U. Jørgensen, B. Amstrup, M. Kmit and and K. S. Mogensen. The operational DMI-HIRLAM system – 2002 version, DMI Tech. Rep., 02–05 (2002) URL: www.dmi.dk/f+u/publikation/tekrap/2002/Tr02-05.pdf

Sattler, K., 1999: *New high resolution physiographic data and climate generation for the HIRLAM forecast system,* DMI Technical report 99-11.

Sattler, K.: 2000, New high resolution physiographic data and climate generation in the HIRLAM forecasting system at DMI, an overview, HIRLAM Newsletter 33, pp.96--100.

Schatzmann, M, and Leitl, B. (2002): Validation and Application of Obstacle Resolving Dispersion Models. *Atmospheric Environment*, Vol.36, pp. 4811-4821.

Schlunzen, H. and J.J. Katzfey, 2003: Relevance of sub-grid-scale land-use effects for mesoscale models. *Tellus,* 55A(3).

Snyder, W.H. 1981: Guideline for Fluid Modelling of Atmospheric Diffusion. US Environmental Protection Agency. EPA-600/8-81-009, 185 S.

Soliman, B.F.: 1976, A study of the wind pressure forces acting on groups of buildings, PhD Thesis, University of Sheffield, UK

Taylor, P., 1987: Comments and further analysis on the effective roughness length for use in numerical 3D models. *Boundary-Layer Metorol.*, **39**, 403-418

Tillman, J.E.: 1972, The indirect determination of stability, heat, and momentum fluxes in the atmospheric boundary layer from simple scalar variables during dry unstable conditions, *J. Appl. Meteorol.*, **11**, 783-792

Undin, P., L. Rontu, H. Järvinen, P. Lynch, J. Calvo, G. Cats, J. Cuhart, K. Eerola, etc., 2002: HIRLAM-5

Scientific Documentation. December 2002, HIRLAM-5 Project Report, SMHI, Norrköping, Sweden.

VDI Richtlinie 3783, Blatt 12 1999: Umweltmeteorologie. Physikalische Modellierung von Strömungs- und Ausbreitungsvorgängen in der Atmosphärischen Grenzschicht. *VDI Handbuch Reinhaltung Luft, Band 1b, Vorentwurf August 1999*

Voogt, J.A. and C.J.B. Grimmond, 2000: Modelling surface sensible heat flux using surface radiative temperatures in a simple urban area. *J. Appl. Meteorol*., **39**, 1679-1699.

Wieringa, J.: 1993, Representative roughness parameters for homogeneous terrain, *Boundary-Layer Metorol.*, **63**, 323-362.

Wood N., Mason P., 1991: The Influence of Static Stability on the Effective Roughness Lengths for Momentum and Heat Transfer. *Q.J.R. Meteorological Society*, Vol 117, pp. 1025-1056.

Zilitinkevich S.S., 1970: Dynamics of the Atmospheric Boundary Layer. Godrometizdat, Leningrad, USSR, (in Russian).

Zilitinkevich S.S., Grachev A.A., C.W. Fairall, 2001: Scaling Reasoning and Field Data on the Sea Surface Roughness Lengths for Scalars. *Journal of Atmospheric Sciences*, Vol 58, pp. 320-325.

Zilitinkevich, S. and A. Baklanov, 2002: Calculation of the height of stable boundary layers in practical applications. *Boundary-Layer Meteorology*, 105(3): 389-409.

Zilitinkevich, S.S., J.C.R. Hunt, A.A. Grachev, I.N. Esau, D.P. Lalas, E. Akylas, C.W. Fairall, H.J.S. Fernando, 2003: Eddy motions and transfer processes at the surface in the shear-free convective boundary layer. Manuscript.

DANISH METEOROLOGICAL INSTITUTE

Scientific Reports

Scientific reports from the Danish Meteorological Institute cover a variety of geophysical fields, i.e. meteorology (including climatology), oceanography, subjects on air and sea pollution, geomagnetism, solar-terrestrial physics, and physics of the middle and upper atmosphere.

Reports in the series within the last five years:

No. 99-1
Henrik Feddersen: Project on prediction of climate variations on seasonel to interannual timescales (PROVOST) EU contract ENVA4-CT95-0109: DMI contribution to the final report: Statistical analysis and post-processing of uncoupled PROVOST simulations

No. 99-2
Wilhelm May: A time-slice experiment with the ECHAM4 A-GCM at high resolution: the experimental design and the assessment of climate change as compared to a greenhouse gas experiment with ECHAM4/OPYC at low resolution

No. 99-3
Niels Larsen et al.: European stratospheric monitoring stations in the Artic II: CEC Environment and Climate Programme Contract ENV4-CT95-0136. DMI Contributions to the project

No. 99-4
Alexander Baklanov: Parameterisation of the deposition processes and radioactive decay: a review and some preliminary results with the DERMA model

No. 99-5
Mette Dahl Mortensen: Non-linear high resolution inversion of radio occultation data

No. 99-6
Stig Syndergaard: Retrieval analysis and methodologies in atmospheric limb sounding using the GNSS radio occultation technique

No. 99-7
Jun She, Jacob Woge Nielsen: Operational wave forecasts over the Baltic and North Sea

No. 99-8
Henrik Feddersen: Monthly temperature forecasts for Denmark - statistical or dynamical?

No. 99-9
P. Thejll, K. Lassen: Solar forcing of the Northern hemisphere air temperature: new data

No. 99-10
Torben Stockflet Jørgensen, Aksel Walløe Hansen: Comment on "Variation of cosmic ray flux and global coverage - a missing link in solar-climate relationships" by Henrik Svensmark and Eigil Friis-Christensen

No. 99-11
Mette Dahl Meincke: Inversion methods for atmospheric profiling with GPS occultations

No. 99-12
Hans-Henrik Benzon; Laust Olsen; Per Høeg: Simulations of current density measurements with a Faraday Current Meter and a magnetometer

No. 00-01
Per Høeg; G. Leppelmeier: ACE - Atmosphere Climate Experiment

No. 00-02
Per Høeg: FACE-IT: Field-Aligned Current Experiment in the Ionosphere and Thermosphere

No. 00-03

Allan Gross: Surface ozone and tropospheric chemistry with applications to regional air quality modeling. PhD thesis

No. 00-04

Henrik Vedel: Conversion of WGS84 geometric heights to NWP model HIRLAM geopotential heights

No. 00-05

Jérôme Chenevez: Advection experiments with DMI-Hirlam-Tracer

No. 00-06

Niels Larsen: Polar stratospheric clouds micro-physical and optical models

No. 00-07

Alix Rasmussen: "Uncertainty of meteorological parameters from DMI-HIRLAM"

No. 00-08

A.L. Morozova: Solar activity and Earth's weather. Effect of the forced atmospheric transparency changes on the troposphere temperature profile studied with atmospheric models

No. 00-09

Niels Larsen, Bjørn M. Knudsen, Michael Gauss, Giovanni Pitari: Effects from high-speed civil traffic aircraft emissions on polar stratospheric clouds

No. 00-10

Søren Andersen: Evaluation of SSM/I sea ice algorithms for use in the SAF on ocean and sea ice, July 2000

No. 00-11

Claus Petersen, Niels Woetmann Nielsen: Diagnosis of visibility in DMI-HIRLAM

No. 00-12

Erik Buch: A monograph on the physical oceanography of the Greenland waters

No. 00-13

M. Steffensen: Stability indices as indicators of lightning and thunder

No. 00-14

Bjarne Amstrup, Kristian S. Mogensen, Xiang-Yu Huang: Use of GPS observations in an optimum interpolation based data assimilation system

No. 00-15

Mads Hvid Nielsen: Dynamisk beskrivelse og hydrografisk klassifikation af den jyske kyststrøm

No. 00-16

Kristian S. Mogensen, Jess U. Jørgensen, Bjarne Amstrup, Xiaohua Yang and Xiang-Yu Huang: Towards an operational implementation of HIRLAM 3D-VAR at DMI

No. 00-17

Sattler, Kai; Huang, Xiang-Yu: Structure function characteristics for 2 meter temperature and relative humidity in different horizontal resolutions

No. 00-18

Niels Larsen, Ib Steen Mikkelsen, Bjørn M. Knudsen m.fl.: In-situ analysis of aerosols and gases in the polar stratosphere. A contribution to THESEO. Environment and climate research programme. Contract no. ENV4-CT97-0523. Final report

No. 00-19

Amstrup, Bjarne: EUCOS observing system experiments with the DMI HIRLAM optimum interpolation analysis and forecasting system

No. 01-01

V.O. Papitashvili, L.I. Gromova, V.A. Popov and O. Rasmussen: Northern polar cap magnetic activity index PCN: Effective area, universal time, seasonal, and solar cycle variations

No. 01-02

M.E. Gorbunov: Radioholographic methods for processing radio occultation data in multipath regions

No. 01-03

Niels Woetmann Nielsen; Claus Petersen: Calculation of wind gusts in DMI-HIRLAM

No. 01-04

Vladimir Penenko; Alexander Baklanov: Methods of sensitivity theory and inverse modeling for estimation of source parameter and risk/vulnerability areas

No. 01-05

Sergej Zilitinkevich; Alexander Baklanov; Jutta Rost; Ann-Sofi Smedman, Vasiliy Lykosov and Pierluigi Calanca: Diagnostic and prognostic equations for the depth of the stably stratified Ekman boundary layer

No. 01-06

Bjarne Amstrup: Impact of ATOVS AMSU-A radiance data in the DMI-HIRLAM 3D-Var analysis and forecasting system

No. 01-07

Sergej Zilitinkevich; Alexander Baklanov: Calculation of the height of stable boundary layers in operational models

No. 01-08

Vibeke Huess: Sea level variations in the North Sea – from tide gauges, altimetry and modelling

No. 01-09

Alexander Baklanov and Alexander Mahura: Atmospheric transport pathways, vulnerability and possible accidental consequences from nuclear risk sites: methodology for probabilistic atmospheric studies

No. 02-01

Bent Hansen Sass and Claus Petersen: Short range atmospheric forecasts using a nudging procedure to combine analyses of cloud and precipitation with a numerical forecast model

No. 02-02

Erik Buch: Present oceanographic conditions in Greenland waters

No. 02-03

Bjørn M. Knudsen, Signe B. Andersen and Allan Gross: Contribution of the Danish Meteorological Institute to the final report of SAMMOA. CEC contract EVK2-1999-00315: Spring-to.-autumn measurements and modelling of ozone and active species

No. 02-04

Nicolai Kliem: Numerical ocean and sea ice modelling: the area around Cape Farewell (Ph.D. thesis)

No. 02-05

Niels Woetmann Nielsen: The structure and dynamics of the atmospheric boundary layer

No. 02-06

Arne Skov Jensen, Hans-Henrik Benzon and Martin S. Lohmann: A new high resolution method for processing radio occultation data

No. 02-07

Per Høeg and Gottfried Kirchengast: ACE+: Atmosphere and Climate Explorer

No. 02-08

Rashpal Gill: SAR surface cover classification using distribution matching

No. 02-09

Kai Sattler, Jun She, Bent Hansen Sass, Leif Laursen, Lars Landberg, Morten Nielsen og Henning S. Christensen: Enhanced description of the wind climate in Denmark for determination of wind resources: final report for 1363/00-0020: Supported by the Danish Energy Authority

No. 02-10

Michael E. Gorbunov and Kent B. Lauritsen: Canonical transform methods for radio occultation data

No. 02-11

Kent B. Lauritsen and Martin S. Lohmann: Unfolding of radio occultation multipath behavior using phase models

No. 02-12

Rashpal Gill: SAR ice classification using fuzzy screening method

No. 02-13

Kai Sattler: Precipitation hindcasts of historical flood events

No. 02-14

Tina Christensen: Energetic electron precipitation studied by atmospheric x-rays

No. 02-15

Alexander Mahura and Alexander Baklanov: Probablistic analysis of atmospheric transport patterns from nuclear risk sites in Euro-Arctic Region

No. 02-16

A. Baklanov, A. Mahura, J.H. Sørensen, O. Rigina, R. Bergman: Methodology for risk analysis based on atmospheric dispersion modelling from nuclear risk sites

No. 02-17

A. Mahura, A. Baklanov, J.H. Sørensen, F. Parker, F. Novikov K. Brown, K. Compton: Probabilistic analysis of atmospheric transport and deposition patterns from nuclear risk sites in russian far east

No. 03-01

Hans-Henrik Benzon, Alan Steen Nielsen, Laust Olsen: An atmospheric wave optics propagator, theory and applications

No. 03-02

A.S. Jensen, M.S. Lohmann, H.-H. Benzon and A.S. Nielsen: Geometrical optics phase matching of radio occultation signals

No. 03-03

Bjarne Amstrup, Niels Woetmann Nielsen and Bent Hansen Sass: DMI-HIRLAM parallel tests with upstream and centered difference advection of the moisture variables for a summer and winter period in 2002

No. 03-04

Alexander Mahura, Dan Jaffe and Joyce Harris: Identification of sources and long term trends for pollutants in the Arctic using isentropic trajectory analysis

No. 03-05

Jakob Grove-Rasmussen: Atmospheric Water Vapour Detection using Satellite GPS Profiling

No. 03-06

Bjarne Amstrup: Impact of NOAA16 and NOAA17 ATOVS AMSU-A radiance data in the DMI-HIRLAM 3D-VAR analysis and forecasting system - January and February 2003

No. 03-07

Kai Sattler and Henrik Feddersen: An European Flood Forecasting System EFFS. Treatment of uncertainties in the prediction of heavy rainfall using
different ensemble approaches with DMI-HIRLAM

No. 03-08

Peter Thejll and Torben Schmith: Limitations on regression analysis due to serially correlated residuals: Application to climate reconstruction from proxies

No. 03-09

Peter Stauning, Hermann Lühr, Pascale Ultré-Guérard, John LaBrecque, Michael Purucker, Fritz Primdahl, John L. Jørgensen, Freddy Christiansen, Per Høeg, Kent B. Lauritsen: OIST-4 Proceedings. 4'th Oersted International Science Team Conference. Copenhagen 23-27 September 2002

No. 03-10

Niels Woetmann Nielsen: A note on the sea surface momentum roughness length.

No. 03-11

Niels Woetmann Nielsen: Quasigeostrophic interpretation of extratropical cyclogenesis

No. 03-12

Alexander Baklanov: FUMAPEX – project kick-off meeting and first progress report. Integrated systems for forecasting urban meteorology, air pollution and population exposure, EVK4-CT-2002-00097

No. 03-13

Rasmus Tonboe, Søren Andersen, Leif Toudal: Anomalous winter sea ice backscatter and brightness temperatures

No. 03-14

Alexander Mahura, Alexander Baklanov, Jens Havskov Sørensen: Long-term probabilistic atmospheric transport and deposition patterns from nuclear risk sites in euro-arctic region. Arctic risk – project of the Nordic Arctic Research Programme (NARP)

No. 03-15

Alexander Mahura, Alexander Baklanov: Evaluation of source-receptor relationship for atmospheric pollutants using trajectory modelling and probability fields analysis

No. 03-16

Niels Woetmann Nielsen, Claus Petersen: A generalized thunderstorm index developed for DMI-HIRLAM

No. 03-17

Jens Havskov Sørensen: Modelling the Atmospheric spread of foot-and mouth disease

No. 03-18

Alexander Baklanov: Evaluation of doses, risks, vulnerabilities and consequences for population and environment in Euro-Arctic Region. Arctic Risk – project of the Nordic Arctic Research Programme (NARP)

No. 03-19

Alexander Baklanov: Improved models for computing the roughness parameters of urban areas. D4.4 FUMAPEX report